# Scattering Calculations with Correlated Gaussians in an Artificial Oscillator Trap

Andreas Mohr Pedersen
201607672


Master's thesis

Supervisor: Dmitri V. Fedorov

Department of Physics and Astronomy
Aarhus University

September 2025

## Colophon

*Scattering Calculations with Correlated Gaussians in an Artificial Oscillator Trap*

Master's thesis by Andreas Mohr Pedersen

The project is supervised by Dmitri V. Fedorov

Typeset by the author using LaTeX and the memoir document class, using Palatino 11.0/14.41597pt.

Printed at Aarhus University

## Abstract

This thesis introduces a new Artificial Confinement Potential (ACP) type recipe for the calculation of low-energy scattering parameters in a quantum few-body system relying exclusively on discrete state calculations. By confining the system in an oscillator trap – characterised by a trap size $b_{\mathrm{o}}$ – the continuum-states are transformed into a quasi-continuum of discrete bound-like states. This enables the use of bound-state methods, such as Explicitly Correlated Gaussians (ECG), in order to calculate the discrete spectrum near threshold. The low-energy scattering parameters – scattering length, effective range and first shape parameter – can be extracted from the discrete spectrum by exploiting its functional dependence upon the trap size. The spectrum and scattering parameters can be related through an analytical formula.

The ACP recipe is tested against a Volkov potential to assess its suitability for practical quantum mechanical few-body calculations. We then apply the ACP recipe to nucleon-nucleon (NN) scattering in the nuclear Model with Explicit Mesons (MEM). We calculate the NN triplet scattering length in the one-sigma approximation ($a = -5.82$ fm) and one-pion approximation ($a = -5.86$ fm). Finally, we attempt to extend the method to nucleon-deuteron scattering in a one-sigma approximation.

Scattering Calculations with Correlated Gaussians in an Artificial Oscillator Trap

## Resume

Denne afhandling introducerer en ny metode baseret på et kunstigt begrænsende potentiale (ACP) til udregning af lavenergispredningsparametre i få-legeme kvantesystemer. Ved at indeslutte systemet i et harmonisk oscillatorpotentiale – karakteriseret af en breddeparameter $b_{\mathrm{o}}$ – transformeres kontinuumtilstandene til et kvasi-kontinuum af tætliggende tilnærmelsesvis bundne tilstande. Dette muliggør anvendelse af velkendte metoder til beregning af bundne tilstande, såsom Eksplicitte Korrelerede Gausser (ECG), til at finde det diskrete spektrum tæt ved tærskelenergien. De tilhørende lavenergispredningsparametre – spredningslængde, effektiv rækkevidde og formparameter – kan da ekstraheres fra den funktionelle afhængighed mellem spektret og størrelsen på oscillatoren. Disse kan relateres via en analytisk formel.

ACP metoden testes på et Volkov-potentiale, for at vurdere, om den er egnet til praktiske beregninger af få-legeme kvantemekaniske systemer. ACP metoden anvendes herefter på nukleon-nukleon spredning i Kernemodellen med eksplisitte mesoner (MEM). Vi beregner NN triplet spredningslængden i én-sigma approksimation ($a = -5.82$ fm) og én-pion approksimation ($a = -5.86$ fm). Slutteligt har vi forsøgt at udvide modellen til nukleon-deuteron spredning én-sigma approksimationen.

# Contents

CHAPTER 1

# Introduction

Calculating quantum scattering observables using bound state methods has been a long-standing goal in few-body physics. While variational approaches, such as the Explicitly Correlated Gaussian (ECG) method, are highly effective for bound-state problems, they cannot be directly applied to scattering states. The fundamental issue is that scattering states are not square-integrable ($L^2$), unlike bound states, which makes traditional variational techniques unsuitable for continuum calculations [1]. This challenge has been addressed by the introduction of a class of methods based on adding an artificial confining potential (ACP) to the scattering Hamiltonian. The ACP discretises the system, effectively turning it into a quasi-continuum of closely spaced bound-like states. The corresponding scattering observables are then retrieved from the discrete spectrum [2, 3, 4, 5, 6].

In this thesis, we introduce a novel approach based on confining the system in a harmonic oscillator potential, characterized by a trap size $b_{\text{o}}$. The general idea is to exploit the functional dependence of the energies in the discrete spectrum upon the trap size to directly extract the low-energy scattering parameters. This rests on the underlying assumption that if two interaction models produce identical discrete energy spectra in an artificial confinement potential, they must have the same scattering parameters. Based on this assumption, we can calculate the discrete spectra for a given interaction model, which may not easily produce the low-energy scattering parameters. We can then extract these by fitting a second model to the discrete spectrum. In particular, we use a zero-range potential implemented as a boundary condition at the origin

as one of the interaction models. We present an analytical formula for the spectrum of the zero-range potential in an oscillator trap.

Our approach differs from existing schemes [7, 8, 9, 10] in that we directly target the low-energy scattering parameters – scattering length, effective range, shape parameter. We confine ourselves to the energy levels near threshold and instead exploit their behaviour under variation of the trap size.

The ACP recipe is first tested against a Volkov potential in a proof of concept calculation. Subsequently, we apply it to the nuclear Model with Explicit Mesons (MEM), where the mesons are treated on equal footing with the nucleons themselves. We calculate the scattering parameters of the deuteron in MEM in a one-sigma and one-pion approximation, respectively. We attempt to extend the method to neutron-deuteron scattering in the one sigma approximation. Some of the results of this thesis were published in [11].

CHAPTER 2

# Theoretical Background

In this chapter, we provide a brief outline of the relevant theoretical material underpinning the numerical methods and their implementation in this thesis.

## 2.1 Notation

We start with a brief introduction to the somewhat unconventional notation of the Explicitly Correlated Gaussians method (ECG). It follows that, introduced in [12], which is consistent across systems with a different number of particles. For an N-particle system, we introduce its position vector

$$\mathbf{r} = \begin{pmatrix} \vec{r}_1 \\ \vec{r}_2 \\ \vdots \\ \vec{r}_N \end{pmatrix}, \tag{2.1}$$

where $\mathbf{r}$ is an N-sized vector and $\vec{r}_i$ is the 3-dimensional position vector of the $i$'th particle of the system. N-sized vectors are written in bold if they contain 3D vectors. 3D vectors are denoted by the usual arrow. If they contain only numbers, they are written in regular font. E.g. the vectors picking out 3D vectors from $\mathbf{r}$ are typically denoted $w$. One common instance of this is using $\vec{r}^2 = \mathbf{r}^\mathsf{T} w w^\mathsf{T} \mathbf{r}$ where $w$ picks out $\vec{r}$ as a linear combinations of the entries in $\mathbf{r}$. For consistency, we will treat scalars as $1 \times 1$-matrices in calculations.

These newly introduced vectors have the following properties

$$\begin{aligned} \mathbf{a}^{\mathsf{T}}\mathbf{b} &= \sum_{i=1}^{N} \vec{a}_i \cdot \vec{b}_i, \\ \mathbf{a}^{\mathsf{T}} A \mathbf{b} &= \sum_{i,j=1}^{N} A_{ij} \vec{a}_i \cdot \vec{b}_j, \end{aligned} \tag{2.2}$$

where $A$ is a size-N symmetric positive-definite matrix [12]. The latter property in (2.2) is known as the quadratic form associated with $A$. In fact, many of the usual properties associated with matrix algebra are inherited by this new formalism. However not all[1], and caution is needed when applied in calculation.

## 2.2 Variational Principle

A popular way to approach quantum few-body problems is by use of variational methods. Such approaches allow for approximate – although sometimes very accurate – determination of the wave function. In this section, we introduce the Ritz variational method. The derivation largely follows that outlined in [13].

Let's consider the discrete eigenvalue spectrum of a quantum mechanical system with Hamiltonian $H$

$$H\psi_n = E_n \psi_n, \qquad n = 0, 1, 2, \ldots \tag{2.3}$$

with energies $E_n$ real and ordered such that $E_0 \leq E_1 \leq \ldots \leq E_n$

Eq. (2.3) is generally difficult to solve. However, the variational principle states that the expectation value of the Hamiltonian for an arbitrary function $|\Psi\rangle$ in the state space of the Hamiltonian is an upper bound to the ground state of the system

$$E = \frac{\langle \Psi | H | \Psi \rangle}{\langle \Psi | \Psi \rangle} \geq E_0. \tag{2.4}$$

Suppose $|\Psi\rangle = |\psi(\alpha)\rangle$ is chosen to depend on a set of parameters $\{\alpha_1, \alpha_2, \ldots, \alpha_N\}$. An approximate solution for the ground-state energy

1 E.g. the identity $(\mathbf{r}^{\mathsf{T}}\mathbf{a})(\mathbf{b}^{\mathsf{T}}\mathbf{r}) \neq \mathbf{r}^{\mathsf{T}}(\mathbf{a}\mathbf{b}^{\mathsf{T}})\mathbf{r}$ does not hold in this formalism

can then be obtained by minimising Eq. (2.4) with respect to parameters $\{\alpha_1, \alpha_2, \ldots, \alpha_N\}$. This approach constitutes the Rayleigh-Ritz variational method.

For practical purposes, trial wave functions are usually constructed as linear combinations of independent basis functions, $\psi_i(\alpha_i)$,

$$|\Psi\rangle = \sum_i^N c_i |\psi_i\left(\alpha_i\right)\rangle, \tag{2.5}$$

where $\{\alpha_i\}$ is the above-mentioned set of variational parameters. In this basis Eq. (2.4) reads

$$E = \frac{\sum_{i,j}^N c_i^* c_j \langle\psi_i|H|\psi_j\rangle}{\sum_{i,j}^N c_i^* c_j \langle\psi_i|\psi_j\rangle} = \frac{c^\dagger \mathcal{H} c}{c^\dagger \mathcal{N} c}, \tag{2.6}$$

where $c$ is an $N$-dimensional column vector and $\mathcal{H}$ and $\mathcal{N}$ are the $N \times N$-dimensional Hamiltonian and overlap matrices

$$\mathcal{H}_{ij} = \langle\psi_i|H|\psi_j\rangle, \qquad \mathcal{N}_{ij} = \langle\psi_i|\psi_j\rangle. \tag{2.7}$$

As $\psi_i$ and $\psi_j$ are not necessarily orthogonal, $\mathcal{N}$ is not guaranteed to be diagonal, but can have non-zero off-diagonal elements.

The coefficients are found by minimising (2.6) with respect to $c$. One can show – by exploiting the hermicity of $\mathcal{H}$ and $\mathcal{N}$ – that the condition $\frac{\partial E}{\partial c} = 0$ is fulfilled exactly when $E$ and $c$ are the eigenvalue and eigenvector solving the generalised eigenvalue problem

$$\mathcal{H} c = E \mathcal{N} c. \tag{2.8}$$

Since the basis functions are linearly independent, the Mini-Max theorem states the $n$'th root, $\epsilon_0 \leq \epsilon_1 \leq \ldots \leq \epsilon_n$, of the ordered solutions to (2.8), is an upper bound to the exact $n$'th eigenvalue of $H$

$$E_0 \leq \epsilon_0, E_1 \leq \epsilon_1 \ldots E_N \leq \epsilon_N. \tag{2.9}$$

In general, there will be $N$ solutions to (2.8), with the $n$'th lowest eigenvalue an upper bound to the corresponding exact $n$'th excited energy of the system [1].

Solving Eq. (2.8) yields the energy spectrum and $c$ coefficients from which the system's wave functions can be constructed.

Suppose we now extend the basis with another trial function,

$$|\Psi'\rangle = \sum_{i}^{N+1} c_i |\psi_i\left(\alpha_i\right)\rangle, \tag{2.10}$$

such that the generalized eigenvalue problem (2.8) has solutions $\epsilon'_0 \leq \epsilon'_1 \leq \ldots \leq \epsilon'_N \leq \epsilon'_{N+1}$. Then

$$\epsilon'_0 \leq \epsilon_0 \leq \epsilon'_1 \leq \epsilon_1 \leq \ldots \leq \epsilon'_N \leq \epsilon_N \leq \epsilon'_{N+1} \tag{2.11}$$

where $\epsilon_1 \leq \epsilon_2 \leq \ldots \leq \epsilon_n$ are the eigenvalues of $H$ in the original basis (2.5). The implication of this result is that extending the basis will always improve the estimates for the N lowest eigenvalues.

## 2.3 Explicitly Correlated Gaussians

As discussed in the previous section, the choice of basis functions is central to theapplication of the Ritz variational method. We employ Explicitly Correlated Gaussians (ECG) as basis functions in this thesis. This is a suitable choice since the Gaussians depend on the square of the distance between particles [1, 13]. In this basis, the independent wave functions are represented by a linear combination of explicitly correlated Gaussians. In position space

$$\langle \mathbf{r}|\psi\rangle = \exp\left(-\sum_{i<j=1}^{N}\left(\frac{\vec{r}_i - \vec{r}_j}{b_{ij}}\right)^2\right), \tag{2.12}$$

where $b_{ij}$ are variational parameters.

The ECG's can be compacted into the form

$$\langle \mathbf{r}|\psi\rangle = e^{-\mathbf{r}^{\mathsf{T}} A \mathbf{r}}, \tag{2.13}$$

where $\mathbf{r} = (\vec{r}_1, \vec{r}_2, \ldots, \vec{r}_N)^{\mathsf{T}}$ is the N-particle coordinate vector and $A$ is an $N \times N$ symmetric positive-definite correlation matrix. $A$ can be written as [14]

$$A = \sum_{i<j=1}^{N} \frac{w_{ij} w_{ij}^{\mathsf{T}}}{b_{ij}^2}. \tag{2.14}$$

where $w_{ij}$ are defined such that

$$w_{ij}^{\mathsf{T}}\mathbf{r} = \vec{r}_i - \vec{r}_j. \tag{2.15}$$

With this choice of $w_{ij}$ (and $A$) the relation between (2.12) and (2.13) is apparent[2]. For clarity, we shall denote the ECG's by their correlation matrix, $|\psi\rangle = |A\rangle$.

The ECG's can be written in a more general form known as shifted correlated Gaussians [12]

$$\langle \mathbf{r}|\psi\rangle = e^{-\mathbf{r}^{\mathsf{T}}A\mathbf{r}+\mathbf{a}^{\mathsf{T}}\mathbf{r}}, \tag{2.16}$$

where $\mathrm{a} = (\vec{a}_1, \vec{a}_2, \ldots \vec{a}_N)^{\mathsf{T}}$ contains shift-vectors $\vec{a}_i$, which are introduced as additional variational parameters. Although these will not be used as basis functions in this thesis, they turn out to be advantageous when calculating matrix elements. Hence, we will use these for derivations, but set the shift vector to $0$ when performing calculations. Shifted ECG's will be denoted by their correlation matrix and shift-vector $|A, \mathbf{a}\rangle$.

In general the choice of ECG's as basis functions has several advantages; In the limit where the number of basis functions becomes large, they form a complete basis. Thus, the energy should converge towards the exact eigenvalue for a systematic increase in the number of basis functions. Further, the matrix elements of the matrices $\mathcal{N}$ and $\mathcal{H}$ are often analytic, which is advantageous for the method to be computationally efficient with a large number of basis functions. In fact, the algebraic complexity is unchanged for calculations with $N \geq 3$. On the downside, ECG's are ill-suited to describe the asymptotic behaviour of a wave function at large distances [1, 13].

## Optimization

The generalised eigenvalue problem is solved using SciPy's eigh function [15]. Choosing suitable parameters is central for the energies to converge. We shall sample parameters quasi-randomly from a low-discrepancy sequence. The width of the Gaussians should reflect the inherent scales of the system, and thus it is advantageous to restrict the sampling to subareas of the parameter space for which this is the case [16]. We will optimise the Gaussian basis element in order to improve

[2] $\mathbf{r}^{\mathsf{T}}A\mathbf{r} = \sum_{i<j=1}^{N} \frac{\mathbf{r}^{\mathsf{T}}w_{ij}w_{ij}^{\mathsf{T}}\mathbf{r}}{b_{ij}^2} = \sum_{i<j=1}^{N} \frac{(\vec{r}_i-\vec{r}_j)\cdot(\vec{r}_i-\vec{r}_j)}{b_{ij}^2} = \sum_{i<j=1}^{N} \frac{(\vec{r}_i-\vec{r}_j)^2}{b_{ij}^2}$

the estimate of the energies using a minimisation routine. The parameters composing the $A_i$ matrices are optimised using the Nelder-Mead downhill simplex method [17]. This is done by choosing[3] $b_{ij} = a_{ij}b$ where $a_{ij}$ are optimization parameters, chosen by the minimizer and $b$ is the scale factor as discussed above. The choice of $b$ does not affect the final energy, but it improves the initial guess required by the minimizer. We can optimise the basis to describe multiple energies at once by minimising their sum to obtain decent basis elements for these states.

## 2.4 Matrix Elements

As discussed, the analytic nature of the matrix elements is one of the advantages of the ECG's. In this section, we present the relevant matrix elements for this thesis. A detailed derivation is available in Appendix A. They can also be found in [12].

The matrix elements were calculated using shifted ECG's introduced in section 2.3. We will, for the most part consider s-waves in this thesis. These can be obtained from the general results by setting the shift vectors to zero [18].

### 2.4.1 Overlap

The most fundamental matrix element is the overlap between two ECG's that make up the overlap matrix $\mathcal{N}$. As we shall see, this result appears in all the remaining matrix elements. Consider two shifted ECG's $|A, \mathbf{a}\rangle$ and $|B, \mathbf{b}\rangle$. Their overlap is then given as

$$\langle A, \mathbf{a}|B, \mathbf{b}\rangle = e^{\left(\frac{1}{4}\mathbf{v}^{\mathsf{T}}R\mathbf{v}\right)}\left(\frac{\pi^N}{\det(A+B)}\right)^{\frac{3}{2}} \equiv M \tag{2.17}$$

where $R = (A+B)^{-1}$, $\mathbf{v} = \mathbf{a} + \mathbf{b}$ and $N = \dim(A)$. For s-waves we simply let $\mathbf{v} \to 0$

$$\langle A|B\rangle \overset{\mathbf{v}\to 0}{=} \left(\frac{\pi^N}{\det(A+B)}\right)^{\frac{3}{2}} \equiv M_0. \tag{2.18}$$

[3] $A_i = \sum_{i<j=1}^{N} \frac{w_{ij}w_{ij}^{\mathsf{T}}}{b_{ij}^2}$

### 2.4.2 Kinetic Energy

The expectation value of the kinetic operator is calculated from the general form

$$\hat{K} = \frac{\partial}{\partial \mathbf{r}} K \frac{\partial}{\partial \mathbf{r}^{\mathsf{T}}}. \tag{2.19}$$

For shifted ECG's $|A, \mathbf{a}\rangle$ and $|B, \mathbf{b}\rangle$ the expectation value becomes

$$\langle B, \mathbf{b}|\hat{K}|A, \mathbf{a}\rangle = \left[6\mathrm{Tr}\left(BKAR\right) + \left(\mathbf{b} - BR\mathbf{v}\right)^{\mathsf{T}} K (\mathbf{a} - AR\mathbf{v})\right] M. \tag{2.20}$$

In the special case of s-waves we set $\mathbf{a} = \mathbf{b} = \mathbf{v} = 0$

$$\langle B|\hat{K}|A\rangle \overset{\mathbf{v}}{=}\overset{\rightarrow}{} {}^{0}\, 6\mathrm{Tr}\left(BKAR\right) M_0 \tag{2.21}$$

### 2.4.3 Harmonic Oscillator

The harmonic oscillator can be expressed on the form

$$V(w^{\mathsf{T}}\mathbf{r}) \propto \mathbf{r}^{\mathsf{T}} w w^{\mathsf{T}} \mathbf{r}, \tag{2.22}$$

The resulting matrix element is

$$\langle B, \mathbf{b}|\mathbf{r}^{\mathsf{T}} w w^{\mathsf{T}} \mathbf{r}|A, \mathbf{a}\rangle = \left(\frac{3}{2} w^{\mathsf{T}} R w + \frac{1}{4} \mathbf{v}^{\mathsf{T}} R w w^{\mathsf{T}} R \mathbf{v}, \right) M \tag{2.23}$$

which in the case of s-waves reduces to

$$\langle B|\mathbf{r}^{\mathsf{T}} w w^{\mathsf{T}} \mathbf{r}|A\rangle \overset{\mathbf{v}\rightarrow 0}{=} \left(\frac{3}{2} w^{\mathsf{T}} R w\right) M_0. \tag{2.24}$$

### 2.4.4 Gaussian Form-Factor

The Gaussian form-factor can be written as

$$V(w^{\mathsf{T}}\mathbf{r}) = \exp\left(-\alpha \mathbf{r}^{\mathsf{T}} w w^{\mathsf{T}} \mathbf{r}\right), \tag{2.25}$$

from which the matrix element can be calculated

$$\begin{aligned}\langle B, \mathbf{b}| \exp\left(-\alpha \mathbf{r}^{\mathsf{T}} w w^{\mathsf{T}} \mathbf{r}\right) |A, \mathbf{b}\rangle \\ = \exp\left(\frac{1}{4} \mathbf{v}^{\mathsf{T}} (B + A + \alpha w w^{\mathsf{T}})^{-1} \mathbf{v}\right) \left(\frac{\pi^N}{\det((B + A + \alpha w w^{\mathsf{T}}))}\right)^{\frac{3}{2}}.\end{aligned} \tag{2.26}$$

For s-waves we let $\mathbf{v} \rightarrow 0$

$$\langle B| \exp\left(-\alpha \mathbf{r}^{\mathsf{T}} w w^{\mathsf{T}} \mathbf{r}\right) |A\rangle \overset{\mathbf{v}\rightarrow 0}{=} \left(\frac{\pi^N}{\det((B + A + \alpha w w^{\mathsf{T}}))}\right)^{\frac{3}{2}}. \tag{2.27}$$

## 2.5 Coordinate Transformation

Since we shall not concern ourselves with systems subjected to external forces, only intrinsic particle interactions need to be considered. It will therefore be advantageous to simplify the system by removing the contribution from the center-of-mass (COM) motion.

This is achieved by transforming from the set of single-particle coordinates $\mathbf{r} = (\vec{r}_1, \vec{r}_2, \ldots, \vec{r}_N)$ to a set of relative coordinates $\mathbf{x} = (\vec{x}_1, \vec{x}_2, \ldots, \vec{x}_N)$. Several choices of relative coordinates exist for such a transformation[1, 13]. Here, we shall employ relative Jacobi coordinates. For an $N$-particle system, coordinates transform as [14]

$$\begin{aligned} \vec{x}_{i<N} &= \frac{\sum_{k=1}^{i} m_k \vec{r}_k}{\sum_{k=1}^{i} m_k} - \vec{r}_{i+1}, \\ \vec{x}_N &= \frac{\sum_{k=1}^{N} m_k \vec{r}_k}{\sum_{k=1}^{N} m_k}, \end{aligned} \tag{2.28}$$

where $\vec{x}_{i<N}$ are the first $N-1$ transformed coordinates depending only on inter-particle distances and $\vec{x}_N$ is the COM coordinate. The COM coordinate can now simply be removed, thus reducing the dimensionality of the problem by 1, and easing the computational load of solving the system numerically. Schematically this transformation is shown in Figure 2.1.

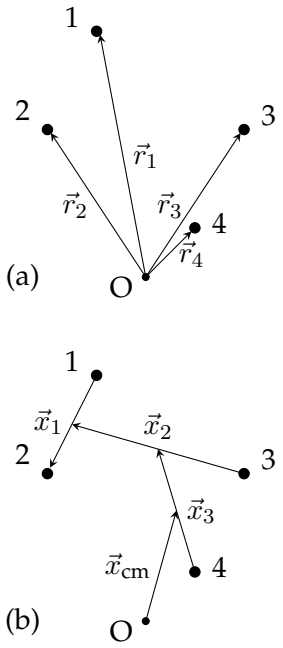


Figure 2.1: A 4-particle system described in different coordinate sets. (a) depicts the system in single particle coordinates, and (b) the same system in Jacobi coordinates.

We can describe the transformation through a matrix $J$[13]

$$\mathbf{r} \to \mathbf{x} = J\mathbf{r}. \tag{2.29}$$

The transformation matrix J is given as

$$J = \begin{pmatrix} 1 & -1 & 0 & \ldots & 0 \\ \frac{m_1}{M_2} & \frac{m_2}{M_2} & -1 & \ldots & 0 \\ \vdots & \vdots & \vdots & \ddots & \vdots \\ \frac{m_1}{M_{N-1}} & \frac{m_2}{M_{N-1}} & \frac{m_3}{M_{N-1}} & \ldots & -1 \\ \frac{m_1}{M_N} & \frac{m_2}{M_N} & \frac{m_3}{M_N} & \ldots & \frac{m_N}{M_N} \end{pmatrix}, \tag{2.30}$$

where $M_i = \sum_{j=1}^{i} m_j$ is the sum of the masses of the first $i$ particles. We shall also be using the inverse of the transformation matrix

$$U = \begin{pmatrix} \frac{m_2}{M_2} & \frac{m_3}{M_3} & \ldots & \frac{m_N}{M_N} & 1 \\ -\frac{M_1}{M_2} & \frac{m_3}{M_3} & \ldots & \frac{m_N}{M_N} & 1 \\ 0 & -\frac{M_2}{M_3} & \ddots & \vdots & \vdots \\ \vdots & \vdots & \ddots & \vdots & \vdots \\ 0 & 0 & \ldots & -\frac{m_{N-1}}{M_N} & 1 \end{pmatrix}. \tag{2.31}$$

As mentioned above, the COM coordinate $\vec{x}_N$ in the transformed system can be removed. This is done by omitting the last row in $J$ or the last column in U.

To preserve the form of the matrix elements under the coordinate transformation, the related matrices and vectors will likewise have to transform[14]. Thus, it remains to be seen how operators and vectors transform under the change of coordinates. The $w$-vectors transforms as[4]

$$w \to U^{\mathsf{T}} w. \tag{2.32}$$

Likewise, the kinetic energy operator $\hat{K} = \frac{\partial}{\partial \mathbf{r}} K \frac{\partial}{\partial \mathbf{r}^{\mathsf{T}}}$ also transforms during the coordinate transformation, since it contains derivatives of the **r**-coordinates. Expanding the quadratic form of $\hat{K}$ as given by (2.2) we see[5]

$$\begin{aligned} \hat{K} &= \frac{\partial}{\partial \vec{r}_i} K_{ij} \frac{\partial}{\partial \vec{r}_j^{\mathsf{T}}} = \frac{\partial}{\partial \vec{x}_k} \frac{\partial \vec{x}_k}{\partial \vec{r}_i} K_{ij} \frac{\partial}{\partial \vec{x}_l} \frac{\partial \vec{x}_l}{\partial \vec{r}_j^{\mathsf{T}}} \\ &= \frac{\partial}{\partial \vec{x}_k} J_{ki} K_{ij} J_{lj} \frac{\partial}{\partial \vec{x}_l} = \frac{\partial}{\partial \vec{x}_k} \left( JKJ^{\mathsf{T}} \right)_{kl} \frac{\partial}{\partial \vec{x}_l} \\ &= \frac{\partial}{\partial \mathbf{x}} JKJ^{\mathsf{T}} \frac{\partial}{\partial \mathbf{x}^{\mathsf{T}}}. \end{aligned} \tag{2.33}$$

Thus, we find that the transformation law for the kinetic energy matrix $K$ is

$$K \to JKJ^{\mathsf{T}}. \tag{2.34}$$

4

$$w^{\mathsf{T}}\mathbf{r} = w^{\mathsf{T}}(U\mathbf{x}) = (w^{\mathsf{T}}U)\mathbf{x} = (U^{\mathsf{T}}w)^{\mathsf{T}}\mathbf{x}$$

5 There is an implicit sum over repeated indices

CHAPTER 3

# Artificial Confinement Potential with a Zero-Range Potential

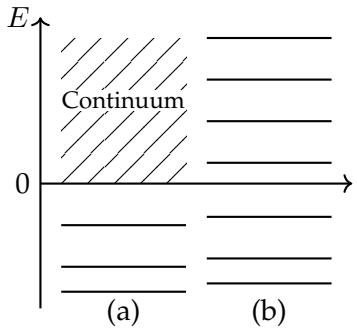


Figure 3.1: (a) shows the energy spectrum of bound- and scattering states. (b) Illustrates the effect of the artificial confinement trap with a harmonic oscillator.

In this section, we introduce a new Artifcial Confinement Potential (ACP) type recipe for the calculation of low-energy scattering parameters. The approach is based on placing the quantum system into an artificial confinement potential – in the form of a harmonic oscillator trap – which turns the scattering states into a quasi-continuum of closely spaced bound-like states (see Figure 3.1).

The corresponding energy spectrum from the quasi-continuum can be calculated using the ECG method. By analysing the bound state energies from the pure oscillator spectrum near the threshold of the system, one should be able to extract the low-energy scattering observables – in particular the scattering length – from its functional dependence upon the trap size, $b_o$. The eigenenergies of the confined system can be related to the low-energy scattering parameters through a zero-range potential model, which we impose as a boundary condition at the origin. With this model, the low-energy scattering parameters of any interaction model can be extracted by fitting the zero-range formula to the energy spectrum of the interaction model. Correspondingly, the energy spectrum $E(b_o)$ of any interaction model can be found for a given set of parameters.

In the following, we introduce the concept of said zero-range potential and subsequently we (re-) derive an analytical formula, relating the discrete eigenenergies of the confined system to the low-energy scattering parameters.

## 3.1 A Zero-Range Potential Boundary Condition

We consider the s-wave radial Schrödinger equation

$$-\frac{\hbar^2}{2m}\frac{\partial^2}{\partial r^2}u\left(r\right)-V\left(r\right)u\left(r\right)=Eu\left(r\right), \tag{3.1}$$

where $u\left(r\right)$ is the radial wave function[1]. $V(r)$ is a short-range potential characterised by a range $b$, such that the potential is negligible when $r>b$. By continuity, the wave function of the inside region ($r<b$) should be 'smoothly' joined with the wave function of the outside region ($r>b$) at the boundary $r=b$. This can be formulated as a boundary condition through the logarithmic derivatives of the inside- and outside solutions[2]

$$\frac{u'_{\text{in}}(b-0)}{u_{\text{in}}(b-0)}=\frac{u'_{\text{out}}(b+0)}{u_{\text{out}}(b+0)}. \tag{3.2}$$

Outside the potential region, the Schrödinger equation simply reads

$$-\frac{\hbar^2}{2m}\frac{\partial^2}{\partial r^2}u\left(r\right)=Eu\left(r\right). \tag{3.3}$$

The solution to Eq. (3.3) is given in the form of a free wave [19, 20] as

$$u_{\text{out}}\left(r\right)=A\sin\left(kr+\delta\right), \tag{3.4}$$

where $\delta$ is the associated phase-shift and $k^2=\frac{2mE}{\hbar^2}$ follows the usual definition. Combining Eq. (3.4) with Eq. (3.2) the boundary condition in the outside region becomes

$$\left.\frac{u'_{\text{out}}}{u_{\text{out}}}\right|_{r=b}=\frac{kA\cos\left(kb+\delta\right)}{A\sin\left(kb+\delta\right)}=k\cot\left(kb+\delta\right). \tag{3.5}$$

We now impose the zero-range potential (ZRP) boundary condition, which effectively corresponds to moving the boundary condition given in Eq. (3.5) to the origin

$$\left.\frac{u'_{\text{out}}}{u_{\text{out}}}\right|_{r=0}=k\cot\left(\delta\right). \tag{3.6}$$

Imposing such an approximation, is expected to be reasonable in the low-energy limit, $kb\ll1$, to which we restrict ourselves in this thesis

1 $\psi\left(r\right)=ru\left(r\right)$[19]

2 The notation $b\pm0$ indicates whether we are slightly inside- or outside the potential.

[21]. In effective-range theory, one oftentimes expands the right-hand side of Eq. (3.6) in a power series around $k^2 = 0$ [22, 23]

$$k \cot(\delta) = \frac{1}{a} + \frac{1}{2} r_e k^2 + P r_e^3 k^4 + O(k^6), \tag{3.7}$$

where $a$ is the scattering length[3], $r_e$ is the effective range and $P$ is known as the first shape parameter.

Combining (3.7) and (3.6), we arrive at the following ZRP-boundary condition at the origin

$$\left. \frac{u'_{\text{out}}}{u_{\text{out}}} \right|_{r=0} = \frac{1}{a} + \frac{1}{2} r_e k^2 + P r_e^3 k^4 + O(k^6), \tag{3.8}$$

which depends on the energy through the usual relation $k^2 = \frac{2mE}{\hbar^2}$.

## 3.2 Harmonic Oscillator with a Zero-Range Potential

We will now derive the zero-range formula (3.8) in a confined system. The derivation of the boundary condition in the previous section was conducted without any additional potential. We now add an artificial confining potential, and so we might consider whether the same boundary condition is still valid. This is indeed the case; one can think of the zero-range potential as the limit where the potential goes to infinity as the range approaches zero (such that the effective range parameters are unchanged). Since the potential is very large in this limit, the addition of any potential finite at the origin does not affect the boundary condition for the zero-range potential. This is especially true in the case of the oscillator, which is zero at the origin.

We thus consider the s-wave radial Schrödinger equation again, but with an additional artificial confinement potential

$$\left( -\frac{\hbar^2}{2m} \frac{d^2}{dr^2} + V(r) + V_{\text{ACP}}(r) \right) u(r) = E u(r), \tag{3.9}$$

where $V(r)$ is, once again, a short range potential; $V_{\text{ACP}}(r)$ is the artificial confinement potential; and $u(r)$ is the radial wave-function.

3 We use the opposite sign convention for $a$

We require a confinement potential with the following properties [3]; $V_{\text{ACP}}(r) \geq E$ for $r \to \infty$; $V_{\text{ACP}}(r)$ should be negligible for $r < b$ where $b$ is the range of the short range potential; and $V_{\text{ACP}}(r)$ should have easily evaluable matrix elements. These conditions are met by the harmonic oscillator, $V_{\text{osc}}(r) = \frac{1}{2}m\omega^2 r^2$, which further benefits from having an evenly spaced spectrum, thus describing the continuum well.

We impose the ZRP boundary condition (see Figure 3.2). Consequently, the short range potential, $V(r)$, disappears entirely from the Schrödinger equation (3.9)

$$\left(-\frac{\hbar^2}{2m}\frac{d^2}{dr^2} + \frac{1}{2}m\omega^2 r^2\right) u(r) = Eu(r). \tag{3.10}$$

Eq. (3.10) can be rewritten on a form known as Weber's equation[4] [24].

$$u''(z) - \left(\alpha + \frac{1}{4}z^2\right) u(z) = 0. \tag{3.12}$$

The solutions to Eq. (3.12) are the so-called parabolic cylinder functions which have the integral representations [25]

$$\begin{aligned} U(\alpha, z) &= \frac{e^{-\frac{1}{4}z^2}}{\Gamma\left(\alpha + \frac{1}{2}\right)} \int_0^\infty e^{-zt} t^{\alpha - \frac{1}{2}} e^{-\frac{1}{2}t^2} dt, \quad \mathcal{R}\alpha > -\frac{1}{2}, \\ U(\alpha, z) &= \sqrt{\frac{2}{\pi}} e^{-\frac{1}{4}z^2} \int_0^\infty \cos(zt + \frac{\pi}{2}\alpha + \frac{\pi}{4}) t^{-\alpha - \frac{1}{2}} e^{-\frac{1}{2}t^2} dt, \quad \mathcal{R}\alpha < \frac{1}{2}. \end{aligned} \tag{3.13}$$

These can be expanded in a power series around $z$

$$U(\alpha, z) = \frac{\sqrt{\pi} 2^{-\frac{\alpha}{2} - \frac{1}{4}}}{\Gamma\left(\frac{\alpha}{2} + \frac{3}{4}\right)} - \frac{\sqrt{\pi} 2^{-\frac{\alpha}{2} - \frac{1}{4}}}{\Gamma\left(\frac{\alpha}{2} + \frac{1}{4}\right)} z + \frac{\sqrt{\pi} 2^{-\frac{\alpha}{2} - \frac{1}{4}}}{\Gamma\left(\frac{\alpha}{2} + \frac{3}{4}\right)} z^2 - \cdots, \tag{3.14}$$

from which we can easily find the values of $U(\alpha, z)$ and $U'(\alpha, z)$ at $z = 0$ which are relevant in our ZRP-model

$$U(\alpha, 0) = \frac{\sqrt{\pi} 2^{\left(-\frac{\alpha}{2} - \frac{1}{4}\right)}}{\Gamma\left(\frac{\alpha}{2} + \frac{3}{4}\right)}, \qquad U'(\alpha, 0) = -\frac{\sqrt{\pi} 2^{\left(-\frac{\alpha}{2} + \frac{1}{4}\right)}}{\Gamma\left(\frac{\alpha}{2} + \frac{1}{4}\right)}. \tag{3.15}$$

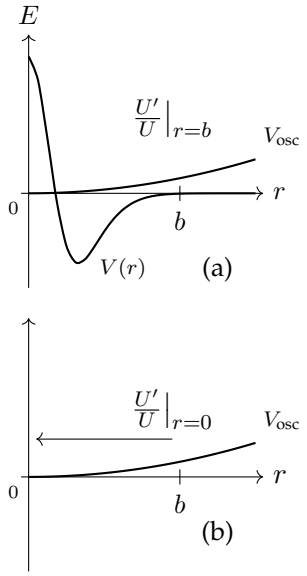


Figure 3.2: Illustration of the system (a) before and (b) after applying the zero-range potential boundary condition.

4 where we have introduced the following variables

$$b_{\text{o}} = \sqrt{\frac{\hbar}{2m\omega}}, \;\; z = \frac{r}{b_{\text{o}}}, \;\; \alpha = -\frac{E}{\hbar\omega}, \tag{3.11}$$

Inserting these on the left side of Eq. (3.8)

$$\frac{1}{b_{\mathrm{o}}}\frac{U'(-\frac{E}{\hbar\omega},0)}{U(-\frac{E}{\hbar\omega},0)} = \frac{1}{a} + \frac{1}{2}\frac{r_{\mathrm{e}}}{b_{\mathrm{o}}^2}\frac{E}{\hbar\omega} + P\frac{r_{\mathrm{e}}^3}{b_{\mathrm{o}}^4}\left(\frac{E}{\hbar\omega}\right)^2, \tag{3.16}$$

where we have used that $k^2 = \frac{E}{b_{\mathrm{o}}^2\hbar\omega}$ and $\frac{d}{dr}\left(U(-\frac{E}{\hbar\omega},\frac{r}{b_{\mathrm{o}}}\right) = \frac{1}{b_{\mathrm{o}}}U'(-\frac{E}{\hbar\omega},\frac{r}{b_{\mathrm{o}}})$. The left-hand side can be expressed through the Gamma-functions[5] of (3.15) resulting in the final expression

$$-\frac{\sqrt{2}}{b_{\mathrm{o}}}\frac{\Gamma\left(-\frac{E}{2\hbar\omega}+\frac{3}{4}\right)}{\Gamma\left(-\frac{E}{2\hbar\omega}+\frac{1}{4}\right)} = \frac{1}{a} + \frac{1}{2}\frac{r_{\mathrm{e}}}{b_{\mathrm{o}}^2}\frac{E}{\hbar\omega} + P\frac{r_{\mathrm{e}}^3}{b_{\mathrm{o}}^4}\left(\frac{E}{\hbar\omega}\right)^2. \tag{3.17}$$

The above expression provides the solutions for the eigenenergies for a zero-range potential in a harmonic oscillator with frequency $\omega$ for a given set of parameters, $a, r_{\mathrm{e}}, P$ and $\omega$. Fitting this equation to an energy spectrum (as a function of $b_{\mathrm{o}}$) of any interaction model, the corresponding low-energy scattering parameters can be obtained.

Equation (3.17) has infinitely many solutions corresponding to the infinite amount of s-wave harmonic oscillations perturbed by the zero-range potential at the origin. The free s-wave oscillator spectrum is restored in the limit $a \to 0$. In this limit, the right-hand side of Eq. (3.17) would be infinite, so the left-hand side must be infinite as well. This is true when the inside of the gamma function in the numerator is a negative integer. Thus, we can obtain the free s-wave spectrum from this condition

$$-\frac{E}{2\hbar\omega} + \frac{3}{4} = -n \qquad \Rightarrow E = \left(2n+\frac{3}{2}\right)\hbar\omega. \tag{3.18}$$

[5] $\frac{U'(\alpha,0)}{U(\alpha,0)} = -\frac{\sqrt{\pi}2^{-\frac{\alpha}{2}+\frac{1}{4}}\Gamma\left(\frac{\alpha}{2}+\frac{3}{4}\right)}{\sqrt{\pi}2^{-\frac{\alpha}{2}-\frac{1}{4}}\Gamma\left(\frac{\alpha}{2}+\frac{1}{4}\right)} = -\sqrt{2}\frac{\Gamma\left(\frac{\alpha}{2}+\frac{3}{4}\right)}{\Gamma\left(\frac{\alpha}{2}+\frac{1}{4}\right)}$

CHAPTER 4

# Test against a Volkov potential

In this Chapter, we perform some preliminary tests on the proposed ACP recipe to assess its suitability for practical calculations in the low-energy regime. We first consider a deuteron in a Volkov potential and extract the resulting scattering parameters. A similar calculation was performed for a Gaussian potential, the results of which can be found in appendix B. We then move on to consider a triton in a Volkov potential to test the viability of the recipe for more complex systems.

## 4.1 Deuteron in a Volkov Potential

We start by considering the theoretical as well as numerical implementation of a deuteron in a Volkov potential (see Figure 4.1) given as [26]

$$W(r) = V_R \exp\left(-\frac{r^2}{R_1^2}\right) + V_A \exp\left(-\frac{r^2}{R_2^2}\right), \tag{4.1}$$

with parameters $V_R = 144.86$ MeV, $R_1 = 0.82$ fm, $V_A = -83.34$ MeV and $R_2 = 1.60$ fm. The model parameters were chosen to reproduce the correct binding energies for $^3$H and $^3$He. As a result, the deuteron is underbound in this parametrisation of the model. The reported binding energy for the deuteron with the above parameters is $-0.546$ MeV.

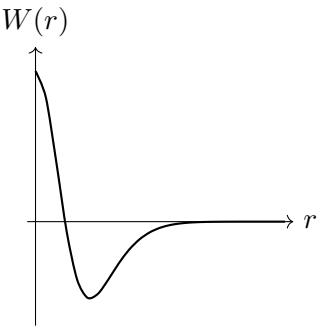

Figure 4.1: Shape of the Volkov potential.

The neutron-proton system can be described by the wave function

$$\Psi = \psi(\mathbf{r}), \tag{4.2}$$

where **r** is the position vector (see Figure 4.2).

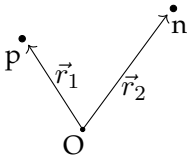


Figure 4.2: Components of **r**.

$$\mathbf{r} = \begin{pmatrix} \vec{r}_1 \\ \vec{r}_2 \end{pmatrix}. \tag{4.3}$$

To calculate the energy spectrum of this system, we need to solve the Schrödinger equation on the general form

$$\hat{H}\Psi = E\Psi. \tag{4.4}$$

As prescribed in chapter 3, we add an artificial oscillator trap to the Hamiltonian. As we are considering a two-particle system, the entire system is placed in the trap, such that the oscillator potential depends on the relative neutron-proton distance. The resulting Hamiltonian is thus given as

$$\hat{H} = -\frac{\partial}{\partial \mathbf{r}} K \frac{\partial}{\partial \mathbf{r}^{\mathsf{T}}} + W(\mathbf{r}) + \frac{1}{4}\frac{\hbar^2}{2\mu b_{\mathrm{o}}^4}(\mathbf{r}^{\mathsf{T}} w w^{\mathsf{T}} \mathbf{r}), \tag{4.5}$$

Where $w = \begin{pmatrix} 1 & -1 \end{pmatrix}^{\mathsf{T}}$ is the vector picking out the relative distance between the neutron and the proton[1]. We assume that $m_n = m_p = \frac{(\hbar c)^2}{41.47\ \text{MeV}\ \text{fm}^2}$ such that the reduced mass $\mu$ is given as in [26]

$$\mu = \frac{1}{2}\frac{(\hbar c)^2}{41.47\ \text{MeV}\ \text{fm}^2} = 469.471\,\text{MeV}. \tag{4.6}$$

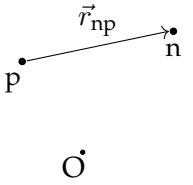


Figure 4.3: The position vector in transformed coordinates.

As no external forces act upon the system, we may benefit from changing into relative Jacobi coordinates. This allows us to disregard the COM coordinate as discussed in section 2.5. Under this transformation (e.g. see Figure 4.3), the transformed position vector $\mathbf{r}_{np}$ follows from Eq. (2.29)

$$\mathbf{r}_{\mathrm{np}} = J\mathbf{r} = \begin{pmatrix} 1 & -1 \end{pmatrix} \begin{pmatrix} \vec{r}_{\mathrm{n}} \\ \vec{r}_{\mathrm{p}} \end{pmatrix} = (\vec{r}_{\mathrm{n}} - \vec{r}_{\mathrm{p}}) = (\vec{r}_{\mathrm{np}}). \tag{4.7}$$

Similarly, the kinetic matrix transforms according to Eq. (2.34)

$$K' = JKJ^T = \begin{pmatrix} 1 & -1 \end{pmatrix} \begin{pmatrix} \frac{\hbar^2}{2m_{\mathrm{n}}} & 0 \\ 0 & \frac{\hbar^2}{2m_{\mathrm{p}}} \end{pmatrix} \begin{pmatrix} 1 \\ -1 \end{pmatrix} = \begin{pmatrix} \frac{\hbar^2}{2\mu} \end{pmatrix}. \tag{4.8}$$

1 $\mathbf{r}^{\mathsf{T}} w w^{\mathsf{T}} \mathbf{r} = |r_2 - r_1|^2$

As such, the Schrödinger equation in relative Jacobi coordinates reads

$$\left[ -\frac{\partial}{\partial \mathbf{r}_{\rm np}} K' \frac{\partial}{\partial \mathbf{r}_{\rm np}^T} + V_R \exp\left( -\frac{\mathbf{r}_{\rm np}^T \tilde{w}\tilde{w}^{\mathsf{T}} \mathbf{r}_{\rm np}}{R_1^2} \right) + V_A \exp\left( -\frac{\mathbf{r}_{\rm np}^T \tilde{w}\tilde{w}^{\mathsf{T}} \mathbf{r}_{\rm np}}{R_2^2} \right) + \frac{1}{4} \frac{\hbar^2}{2\mu b_{\rm o}^4} (\mathbf{r}_{\rm np}^T \tilde{w}\tilde{w}^{\mathsf{T}} \mathbf{r}_{\rm np}) \right] \Psi = E\Psi. \tag{4.9}$$

where $\tilde{w}$ is the $w$-vector transformed according to Eq. (2.32).

We solve this system by means of the Ritz-variational method. The wave function, (4.2), is expanded in a correlated Gaussian basis

$$\psi(\mathbf{r}) = \sum_{i=1}^{N} c_i \exp\left(\mathbf{r}^T A_i \mathbf{r}\right) = \sum_{i=1}^{N} c_i |A_i\rangle, \tag{4.10}$$

from which we calculate the relevant Hamiltonian and overlap matrices. The overlap matrix in the neutron-proton system has entries

$$\mathcal{N}_{ij} = \langle A_i | A_j \rangle = M_0. \tag{4.11}$$

For the Hamiltonian, the entries are given as

$$\mathcal{H}_{ij} = \langle \psi_i | \hat{H} | \psi_j \rangle = \langle A_i | \hat{K} + W + V_{\rm osc} | A_j \rangle, \tag{4.12}$$

resulting in the three matrix elements

$$\langle A_i | \hat{K} | A_j \rangle, \quad \langle A_i | W | A_j \rangle, \quad \langle A_i | V_{\rm osc} | A_j \rangle. \tag{4.13}$$

Their formulae were presented in section 2.4.

### 4.1.1 Spectrum of a Deuteron in a Volkov Potential

The numerically calculated spectrum near threshold as a function of the trap size, $b_{\rm o}$, for the deuteron in a Volkov potential is shown in Figure 4.4. The system was solved with $16$ Gaussians optimised for the ground and first excited state.

The low-energy scattering parameters were extracted by fitting the energies of the ground and first excited states from the last two fermi to Eq. 3.17. The resulting value for the scattering length, $10.08$ agrees very well with the value suggested in [26]. Inspection of Figure 4.4 shows

good agreement between the two interaction models – ZRP and Volkov – with the zero-range model able to reproduce the spectrum for the four lowest energy levels as indicated by the solid lines.

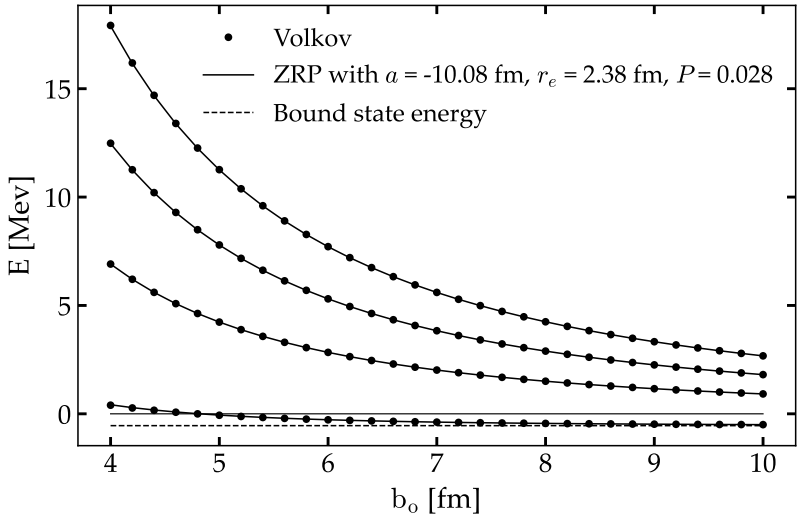


Figure 4.4: Volkov interaction model against the ZRP-model: The dots show the spectrum for a deuteron in a Volkov potential and an oscillator trap as a function of the trap size, $b_o$. The solid lines show the corresponding eigenenergies of the same system interacting through a zero-range potential, Eq. (3.17), with $a = 10.08$, $r_e = 2.38$ and $P = 0.028$. The dashed line indicates the bound state energy of the deuteron. The solid line at $0$ indicates the threshold.

The validity of the results is underlined by the convergence behaviour of the scattering parameters as a function of the trap size. We expect the scattering length to converge towards the value reported in [26], $10.08$ fm, as $b_o$ increases. The results for the convergence with respect to $b_o$ are shown in Figure 4.5.

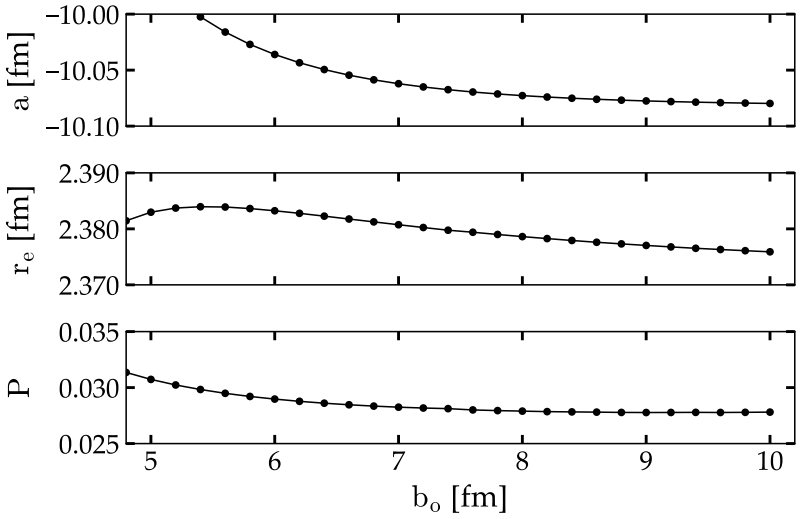


Figure 4.5: Parameter convergence with respect to trap size: each point represents the parameters fitted to the energies of the preceding two fermi. The solid line is included to indicate the trend of the convergence behaviour.

### Inclusion of the Shape Parameter

Oftentimes, the shape parameter is excluded in the effective range expansion, Eq. (3.8). To get a sense of the effect of including it, we have fitted the above spectrum for different orders in the expansion. The resulting parameters are shown in Table 4.1.

| | $a$ [fm] | $r_e$ [fm] | $P$ |
|---|---|---|---|
| 1st order | $-11.14$ | | |
| 2nd order | $-10.09$ | 2.39 | |
| 3rd order | $-10.08$ | 2.38 | 0.028 |

Table 4.1: Scattering parameters for different orders of expansion in the effective range formula, Eq. (3.17).

The 2nd and 3rd order expansions both provide decent values for the scattering length and effective range, suggesting that perhaps two terms in the expansion suffice to extract the scattering parameters. However, the inclusion of P was found to slightly improve the convergence for the remaining parameters, in particular for the effective range, demanding a smaller $b_o$ for convergence. A figure comparing the convergence behaviour of the 2nd and 3rd-order expansions can be found in appendix C.

## 4.2 Triton in a Volkov potential

We now consider a triton in a Volkov potential to test the ACP recipe against a system of added complexity. The Volkov potential is again parametrised as in [26]. Recall that these parameters were chosen to reproduce the correct binding energy for $^3$H and $^3$He. The binding energies for the two lowest energy states in the triton in this parametrisation are $E_0 = -8.432$ MeV and $E_1 = -0.599$.

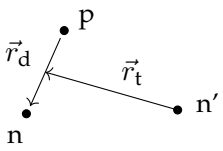


Figure 4.6: Transformed position vector for the triton.

The Triton consist of three nucleons, two neutrons and a proton.

$$\mathbf{r} = \begin{pmatrix} \vec{r}_\mathrm{n} \\ \vec{r}_\mathrm{p} \\ \vec{r}_{\mathrm{n}'} \end{pmatrix}. \tag{4.14}$$

The two-particle model from the previous section is fairly easily extended to accommodate the additional neutron. The position vector changes by one dimension due to the additional neutron

The position vector in relative Jacobi coordinates is thus a two-component structure.

$$\mathbf{r}_{\mathrm{npn}'} = \begin{pmatrix} \vec{r}_\mathrm{d} \\ \vec{r}_\mathrm{t} \end{pmatrix}, \tag{4.15}$$

with components

$$\vec{r}_\mathrm{d} = \left(\vec{r}_\mathrm{n} - \vec{r}_\mathrm{p}\right), \qquad \vec{r}_\mathrm{t} = \left(\frac{m_\mathrm{n}\vec{r}_\mathrm{n} + m_\mathrm{p}\vec{r}_\mathrm{p}}{m_\mathrm{n} + m_\mathrm{p}} - \vec{r}_{\mathrm{n}'}\right), \tag{4.16}$$

where $\vec{r}_\mathrm{d}$ represents the relative distance between the proton and neutron (n) and $\vec{r}_\mathrm{t}$ is the relative distance between the incoming neutron (n′) and the COM of the pn-system (see Figure 4.6).

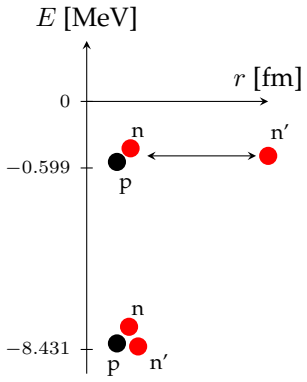


Figure 4.7: Threshold of the neutron-deuteron scattering system [26].

For the triton, we have to reconsider the interaction between the system and the oscillator trap, as compared to the two-particle case. Since we consider a neutron scattering of a deuteron, the interaction with the oscillator trap should be determined by the relative distance between the incoming neutron and the deuteron COM coordinate. Thus, the threshold of the system becomes the bound state energy of the deuteron. To see this, one can consider the case where the neutron is moved infinitely apart from the deuteron, such that only the deuteron contributes to the energy of the system (see Figure 4.7). A vector that

picks out the relative distance between the neutron and the neutron-proton COM can be written as

$$w_{\text{osc}} = \begin{pmatrix} \frac{m_{\text{n}}}{m_{\text{n}}+m_{\text{p}}} \\ \frac{m_{\text{p}}}{m_{\text{n}}+m_{\text{p}}} \\ -1 \end{pmatrix}. \tag{4.17}$$

This vector will likewise have to transform according to Eq. (2.32)

$$\tilde{w}_{\text{osc}} = U^{\mathsf{T}} w_{\text{osc}} = \begin{pmatrix} 0 \\ 1 \end{pmatrix}. \tag{4.18}$$

The corresponding Schrödinger equation for a triton in a Volkov potential plus an oscillator trap can thus be written as

$$\left[ -\frac{\partial}{\partial \mathbf{r}_{\text{npn}'}} K' \frac{\partial}{\partial \mathbf{r}_{\text{npn}'}^{\mathsf{T}}} + \sum_{i=1}^{3} \left\{ V_R \exp\left( -\frac{\mathbf{r}_{\text{npn}'}^{\mathsf{T}} \tilde{w}_i \tilde{w}_i^{\mathsf{T}} \mathbf{r}_{\text{npn}'}}{R_1^2} \right) + V_A \exp\left( -\frac{\mathbf{r}_{\text{npn}'}^{\mathsf{T}} \tilde{w}_i \tilde{w}_i^{\mathsf{T}} \mathbf{r}_{\text{npn}'}}{R_2^2} \right) \right\} + \frac{1}{4} \frac{\hbar^2}{2\mu b_{\text{o}}^4} \left( \mathbf{r}_{\text{npn}'}^{\mathsf{T}} \tilde{w}_{\text{osc}} \tilde{w}_{\text{osc}}^{\mathsf{T}} \mathbf{r}_{\text{npn}'} \right) \right] \Psi = E\Psi. \tag{4.19}$$

where $b_{\text{o}}$ is the trap size and $\mu$ is the reduced mass of the system; $\tilde{w}_i$ are the transformed $w_i$-vectors picking out the relative distance between particles in the system[2].

### 4.2.1 Spectrum of a Triton in a Volkov Potential

The energy spectrum is calculated by numerically solving the Schrödinger equation (4.19) using the ECG method. Due to the added complexity of the system, more Gaussians are needed for the energies of the system to converge. The spectrum was calculated for a total of 200 Gaussians, the parameters of which were optimised by minimising the sum of the ground, 1st, and 2nd excited states.

The resulting eigenenergy spectrum as a function of the trap size, $b_{\text{o}}$, is presented in Figure 4.8. The low-energy scattering parameters were extracted from the last two fermi of the 1st excited state by fitting to Eq.

[2]

$$w_1 = \begin{pmatrix} 1 \\ -1 \\ 0 \end{pmatrix}, \qquad w_2 = \begin{pmatrix} 1 \\ 0 \\ -1 \end{pmatrix}, \qquad w_3 = \begin{pmatrix} 0 \\ 1 \\ -1 \end{pmatrix} \tag{4.20}$$

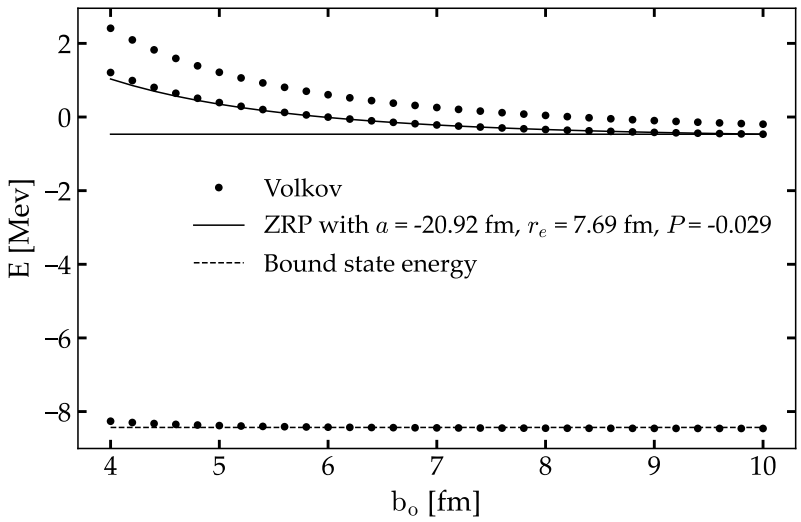


Figure 4.8: The spectrum of a triton in a Volkov potential and an oscillator trap as a function of the trap range, $b_o$, is shown by the dots. The corresponding spectrum for the same particle in the trap with the zero-range potential, Eq. (3.17), with $a = -20.92$ fm, $r_e = 7.69$ fm and $P = -0.029$ is indicated by the solid lines. The dashed line indicates the bound state energy of the triton as in [26]. The horizontal line just below 0 indicates the threshold.

(3.17). The energies used in the fit have to be taken with respect to the threshold of the system, since Eq. (3.17) is a Taylor expansion at $E \to 0$. In figure 4.8, the threshold was set at the final energy of the first excited level. This value converges towards the true bound state energy of the deuteron in the limit where $b_o$ becomes large.

The extracted scattering parameters for the triton system were

$$a = -20.92 \text{ fm}, \quad r_e = 7.69 \text{ fm}, \quad P = -0.029.$$

We may not expect the Volkov potential to provide realistic parameters for the triton that are comparable with experimental values. No calculation of the scattering parameters for the triton in a Volkov potential exists in the literature, such that the scattering parameters can be compared.

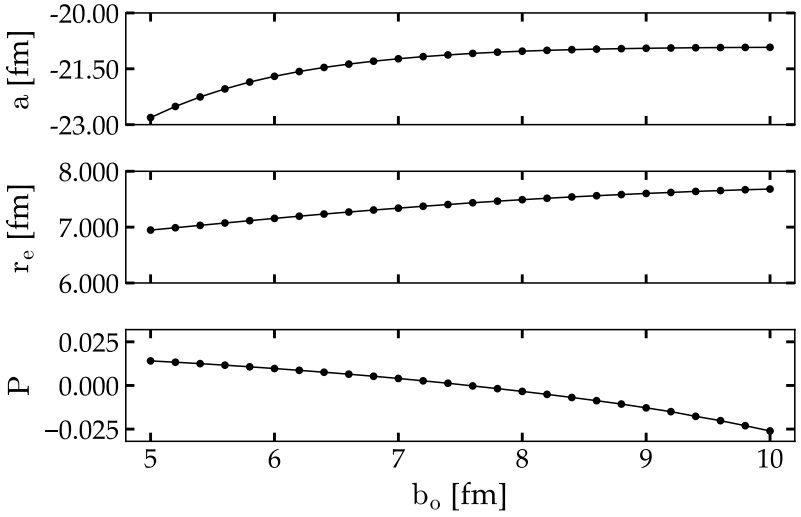


Figure 4.9: Convergence of scattering parameters with respect to the trap size; each point – representing a parameter – is fitted across the energies of the preceding two fermi. The trend of convergence is indicated by the solid lines.

The zero-range formula is only able to reproduce the spectrum for the first excited state for the fitted parameters; however, they have seemingly converged for the scattering length and effective range as seen from Figure 4.9.

## Optimized Threshold

The scattering observables are very susceptible to the value of the threshold. As a test, we now try to include the threshold as a parameter in Eq. (3.17), in order to find an optimal threshold value[3]. The results are presented in Figure 4.10.

The parameters are extracted from the first excited state in the same manner as above. The resulting parameters

$$a = -20.12 \text{ fm}, \quad r_e = 7.65 \text{ fm}, \quad P = -0.033, \quad E_t = -0.450 \text{ MeV}.$$

indicating an optimal threshold slightly above the final energy of the spectrum. This seems somewhat counterintuitive as we would expect

3

$$-\frac{\sqrt{2}}{b_o}\frac{\Gamma\left(-\frac{E-E_t}{2\hbar\omega}+\frac{3}{4}\right)}{\Gamma\left(-\frac{E-E_t}{2\hbar\omega}+\frac{1}{4}\right)} = \frac{1}{a} + \frac{1}{2}\frac{r_e}{b_o^2}\frac{E-E_t}{\hbar\omega} + P\frac{r_e^3}{b_o^4}\left(\frac{E-E_t}{\hbar\omega}\right)^2 \tag{4.21}$$

the energy curve to converge towards the threshold for increasing $b_o$'s. The difference between the threshold values is on the 2nd decimal and does not have a great effect on the accompanying scattering parameters.

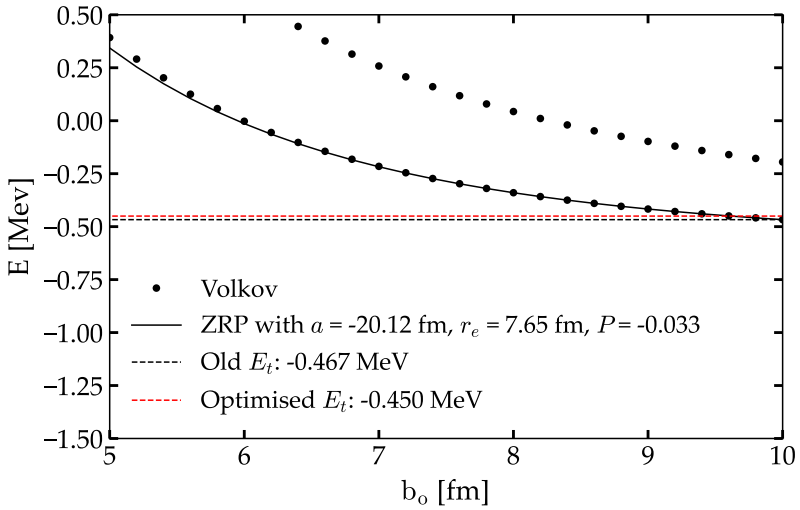


Figure 4.10: Dots: Spectrum of the triton in a Volkov potential. Solid lines: spectrum in the zero-range formula with $a = -20.12$ fm, $r_e = 7.65$ fm, $P = -0.033$, $E_t = -0.450$ MeV. The optimised threshold is indicated by the dashed red line. The old threshold is indicated by the black dashed line.

CHAPTER 5

# Scattering in a Nuclear Model with Explicit Mesons

Having tested our recipe on some simple interaction models, we now turn to apply it to more realistic models. In this chapter, we apply the recipe to the Nuclear model of Explicit Mesons (MEM). MEM differs from conventional potential models in that it applies a direct meson exchange paradigm to describe the low-energy nucleon-nucleon (NN) interaction. That is, the mesons emitted and absorbed between the nucleons are treated analogously to the nucleons themselves [14].

The wave function in the MEM can be represented as a multicomponent structure

$$\Psi = \begin{pmatrix} \psi_{\mathrm{NN}'} \\ \psi_{\mathrm{NN}'\mathrm{M}} \\ \psi_{\mathrm{NN}'\mathrm{MM}'} \\ \vdots \end{pmatrix}, \tag{5.1}$$

where the nucleons N are dressed with virtual mesons M. $\psi_{\mathrm{NN}'}$ represents the bare nucleus, and the subsequent entries in (5.1) are the wave functions dressed with an increasing number of M-mesons.

The Hamiltonian acting on (5.1) is a block-matrix of the same dimen-

sion as the wave function

$$\hat{H} = \begin{pmatrix} \hat{K}_{\mathrm{N}} + \hat{K}_{\mathrm{N}'} + m_{\mathrm{N}} + m_{\mathrm{N}'} & W^{\dagger} & 0 & \cdots \\ W & \hat{H}_{00} + \hat{K}_{\mathrm{M}} + m_{\mathrm{M}} & W^{\dagger} & \cdots \\ 0 & W & \hat{H}_{11} + \hat{K}_{\mathrm{M}} + m_{\mathrm{M}'} & \cdots \\ \vdots & \vdots & \vdots & \ddots \end{pmatrix}, \tag{5.2}$$

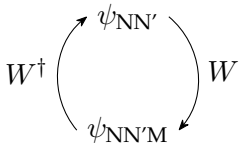


Figure 5.1: Coupling between the bare nucleon state and one mesons state.

where $\hat{K}_N$ and $\hat{K}_M$ are the kinetic energy operator of the nucleons and mesons; $m_N$ and $m_M$ is the masses; $W/W^{\dagger}$ are creation/annihilation operators coupling the two subsystems by creating or annihilating a meson (see Figure 5.1). The corresponding Schrödinger equation takes the usual form

$$H\Psi = E\Psi. \tag{5.3}$$

The nucleon masses can be subtracted from the Hamiltonian (5.2) to leave the resulting energy equal to the binding energy of the system.

The kinetic energy operator for an N-body system is given as

$$\hat{K} = -\sum_{i=1}^{N} \frac{\hbar^2}{2m_i} \frac{\partial^2}{\partial \vec{r}_i^{\,2}}, \tag{5.4}$$

which, for completeness, can be rewritten in the general form

$$\hat{K} = -\frac{\partial}{\partial \mathbf{r}} K \frac{\partial}{\partial \mathbf{r}^T}, \tag{5.5}$$

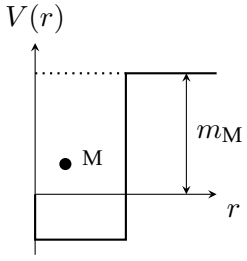


Figure 5.2: Virtual meson trapped under a potential barrier.

where

$$K_{ii} = \frac{\hbar^2}{2m_i} \tag{5.6}$$

is a diagonal matrix.

The mesons will reside under a potential barrier, the size of their combined masses, and are considered virtual unless the needed amount of energy is supplied to the system as shown in Figure 5.2 [14, 27]. We can thus safely assume that the first virtual meson will be responsible for the largest contribution to the dressing of the bare nucleus and restrict ourselves to the one-meson approximation going forward.

## 5.1 Neutron-Proton Scattering in $\sigma$MEM

We first consider MEM in its simplest form with a single scalar-isoscalar $\sigma$-meson. $\sigma$MEM has already successfully reproduced the deuteron binding energy and charge radius [14]. Our proposed recipe provides a test for the corresponding scattering observables. In this section, we calculate the triplet NN scattering length and effective range.

### 5.1.1 One-Sigma Approximation

The total wave function of the deuteron is a two-component structure

$$\Psi = \begin{pmatrix} \psi_{\mathrm{np}}(\mathbf{r}_{\mathrm{np}}) \\ \psi_{\mathrm{np}\sigma}(\mathbf{r}_{\mathrm{np}\sigma}) \end{pmatrix}. \tag{5.7}$$

The first entry is referred to as the np-system and the second entry as the $\sigma$-system. $\mathbf{r}_{\mathrm{np}}$ and $\mathbf{r}_{\mathrm{np}\sigma}$ are the position vectors of the respective subsystems

$$\mathbf{r}_{\mathrm{np}} = \begin{pmatrix} \vec{r}_{\mathrm{n}} \\ \vec{r}_{\mathrm{p}} \end{pmatrix}, \qquad \mathbf{r}_{\mathrm{np}\sigma} = \begin{pmatrix} \vec{r}_{\mathrm{n}} \\ \vec{r}_{\mathrm{p}} \\ \vec{r}_{\sigma} \end{pmatrix}. \tag{5.8}$$

From Eq. (5.2) the corresponding Hamiltonian becomes

$$\hat{H} = \begin{pmatrix} \hat{K}_{\mathrm{n}} + \hat{K}_{\mathrm{p}} + V_{\mathrm{osc}} & W^{\dagger} \\ W & \hat{K}_{\mathrm{n}} + \hat{K}_{\mathrm{p}} + \hat{K}_{\sigma} + m_{\sigma} \end{pmatrix}, \tag{5.9}$$

where the masses of the neutron and the proton have been subtracted from the diagonal; $\hat{K}_{\mathrm{n}},\ \hat{K}_{\mathrm{p}},\ \hat{K}_{\sigma}$ are the kinetic energy operators; $m_{\sigma}$ is the mass of the sigma-meson; $W/W^{\dagger}$ are the coupling operators creating and annihilating a $\sigma$-meson; $V_{\mathrm{osc}}$ is the artificial oscillator trap.

Note that we only need to confine the np-system, since, at the energies involved – just above the np-threshold – the sigma-meson is in the classically forbidden region and the $\sigma$-system is in a sense self-confined; there is no need for a trap. Only at energies above the $\sigma$ threshold, 500 MeV would we need to confine the $\sigma$-system as well.

The coupling operator can be introduced on the integral form [14]

$$\langle \psi_{\mathrm{np}} | W | \psi_{\mathrm{np}\sigma} \rangle = \int d\mathbf{r}^3_{\mathrm{np}} d\mathbf{r}^3_{\mathrm{np}\sigma} \psi^*_{\mathrm{np}} W \left( \mathbf{r}_{\mathrm{np}}, \mathbf{r}_{\mathrm{np}\sigma} \right) \psi_{\mathrm{np}\sigma}. \tag{5.10}$$

$W\left(\mathbf{r}_{\mathrm{np}}, \mathbf{r}_{\mathrm{np}\sigma}\right)$ must be short-ranged and vanish at large inter-particle distances. This is conveniently achieved by a Gaussian-type operator

$$W\left(\mathbf{r}_{\mathrm{np}}, \mathbf{r}_{\mathrm{np}\sigma}\right) = S_\sigma \exp\left(-\frac{\mathbf{r}_{\mathrm{np}}^2 + \mathbf{r}_{\mathrm{np}\sigma}^2}{b_\sigma^2}\right). \tag{5.11}$$

where $b_\sigma$ is the range and $S_\sigma$ the strength parameter of the model. For the deuteron in the one-sigma approximation, the appropriate parameters are

$$S_\sigma = 20.35 \text{ MeV}, \qquad b_\sigma = 3 \text{ fm} \tag{5.12}$$

which reproduce the correct values for the binding energy and charge radius [14].

As we did for the potential models, we transform into relative Jacobi coordinates. The position vectors transform according to (2.29)

$$\mathbf{r}_{\mathrm{np}} \to \mathbf{r}_{\mathrm{d}} = \left(\vec{r}_{\mathrm{n}} - \vec{r}_{\mathrm{p}}\right), \qquad \mathbf{r}_{\mathrm{np}\sigma} \to \mathbf{r}_\sigma = \begin{pmatrix} \vec{r}_{\mathrm{n}} - \vec{r}_{\mathrm{p}} \\ \frac{m_{\mathrm{n}}\vec{r}_{\mathrm{n}} + m_{\mathrm{p}}\vec{r}_p}{m_{\mathrm{n}}+m_{\mathrm{p}}} - \vec{r}_\sigma \end{pmatrix}. \tag{5.13}$$

The kinetic energy operators in the transformed coordinates become

$$\hat{K}_{\mathrm{d}} = \frac{\partial}{\partial \mathbf{r}_{\mathrm{d}}} K_{\mathrm{d}} \frac{\partial}{\partial \mathbf{r}_{\mathrm{d}}^\intercal}, \qquad \hat{K}_\sigma = \frac{\partial}{\partial \mathbf{r}_\sigma} K_\sigma \frac{\partial}{\partial \mathbf{r}_\sigma^\intercal}, \tag{5.14}$$

with

$$K_{\mathrm{d}} = \left(\tfrac{\hbar^2}{2\mu_{\mathrm{d}}}\right), \qquad K_\sigma = \begin{pmatrix} \frac{\hbar^2}{2\mu_{\mathrm{d}}} & 0 \\ 0 & \frac{\hbar^2}{2\mu_\sigma} \end{pmatrix}, \tag{5.15}$$

where $\mu_{\mathrm{d}}$ and $\mu_\sigma$ are the reduced masses of the system. The resulting Schrödinger equation can be written as a coupled system of equations

$$\begin{cases} \left(\frac{\partial}{\partial \mathbf{r}_{\mathrm{d}}} K_{\mathrm{d}} \frac{\partial}{\partial \mathbf{r}_{\mathrm{d}}^\intercal} + V_{\mathrm{osc}}\right) \psi_{\mathrm{d}} + W^\dagger \psi_\sigma = E \psi_{\mathrm{d}} \\ W \psi_{\mathrm{d}} + \left(\hat{K}_\sigma + m_\sigma\right) \psi_\sigma = E \psi_\sigma. \end{cases} \tag{5.16}$$

We will very briefly summarise the theoretical setup applied to $\sigma$MEM. The wave functions are

$$\psi_{\mathrm{d}} = \sum_{i=1}^{N_{\mathrm{d}}} c_i \exp\left(-\mathbf{r}_{\mathrm{d}}^\intercal A_i^{\mathrm{d}} \mathbf{r}_{\mathrm{d}}\right), \qquad \psi_\sigma = \sum_{j=1}^{N_\sigma} c_j \exp\left(-\mathbf{r}_\sigma^\intercal A_j^\sigma \mathbf{r}_\sigma\right). \tag{5.17}$$

The Hamiltonian and overlap matrices are $2 \times 2$ block matrices

$$\mathcal{H} = \begin{pmatrix} \langle A_i^d | \hat{K}_{\mathrm{d}} | A_j^{\mathrm{d}} \rangle & \langle A_i^{\mathrm{d}} | W^\dagger | A_j^\sigma \rangle \\ \langle A_i^\sigma | W | A_j^{\mathrm{d}} \rangle & \langle A_i^\sigma | \hat{K}_\sigma | A_j^\sigma \rangle \end{pmatrix}, \qquad \mathcal{N} = \begin{pmatrix} \langle A_i^{\mathrm{d}} | A_j^{\mathrm{d}} \rangle & 0 \\ 0 & \langle A_i^\sigma | A_j^\sigma \rangle \end{pmatrix}. \tag{5.18}$$

The relevant matrix elements were all introduced in section 2.4. The $\langle A_i^\sigma | W | A_j^{\mathrm{d}} \rangle$ matrix element can be written in a simpler form,

$$\langle A_i^\sigma | W | A_j^{\mathrm{d}} \rangle = S_\sigma \langle \tilde{A}_i^\sigma | A_j^{\mathrm{d}} \rangle \tag{5.19}$$

with

$$\tilde{A}_i^\sigma = \begin{pmatrix} A_i^\sigma + \frac{1}{b_\sigma^2} & 0 \\ 0 & \frac{1}{b_\sigma^2} \end{pmatrix}. \tag{5.20}$$

### 5.1.2 $\sigma$MEM Spectrum

The spectrum of eigenenergies for the $\sigma$MEM is shown in Figure 5.3. The parameters of the Gaussians are optimised by minimising the sum of the ground and first excited state with $15$ Gaussians in the np-system and $50$ Gaussians in the $\sigma$-system. The mass of the of the nucleons were set at $m_{\mathrm{p}} = m_{\mathrm{n}} = 939$ MeV and the mass of the $\sigma$-meson was set at $m_\sigma = 500$ MeV. The final two fermi of the two energy levels closest to the threshold of the system were used to extract the parameters. The low-energy scattering parameters were found to be

$$a = -5.82 \text{ fm}, \quad r_e = 2.23 \text{ fm}, \quad P = 0.13,$$

for the $\sigma$MEM. Although these would seem qualitatively correct, since the ZRP model can reproduce the energy spectrum, there is some discrepancy when compared with the experimental values. These, for the deuteron triplet, ${}^3S_1$, are [28]

$$a = -5.4112(15) \text{ fm}, \qquad r_{\mathrm{e}} = 1.7436(19) \text{ fm}.$$

We see that the $\sigma$MEM overestimates the scattering parameters for the scattering length and effective range. Evidently, the one-sigma approximation is not sufficient. The convergence of the resulting parameters with respect to the trap size is shown in Figure 5.4.

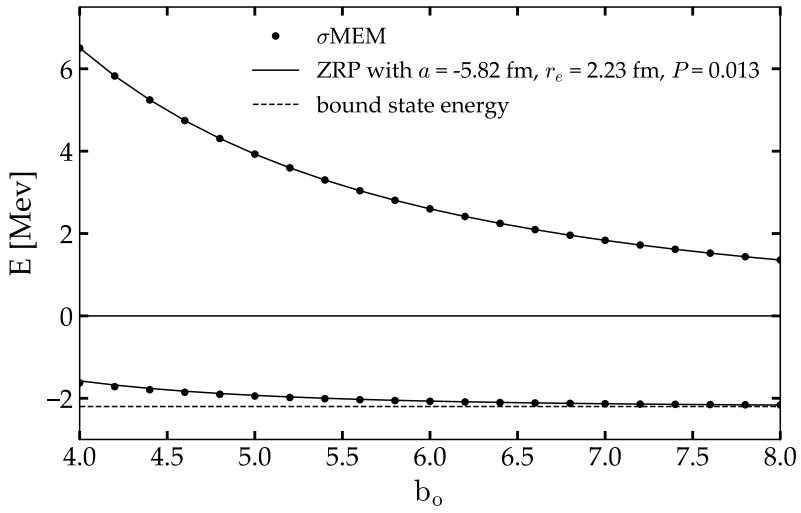


Figure 5.3: The dots show the spectrum for the two lowest eigenenergies for the neutron-proton system in an oscillator trap calculated in $\sigma$MEM, Eq. (5.16). The corresponding eigenenergies calculated for the neutron-proton system in an oscillator trap with a zero-range potential, Eq. (3.17), with $a = -5.82$ MeV, $r_e = 2.23$ fm and $P = 0.013$. The dotted line indicates the bound state energy of the deuteron given in [14]. The solid line at 0 indicates the system threshold.

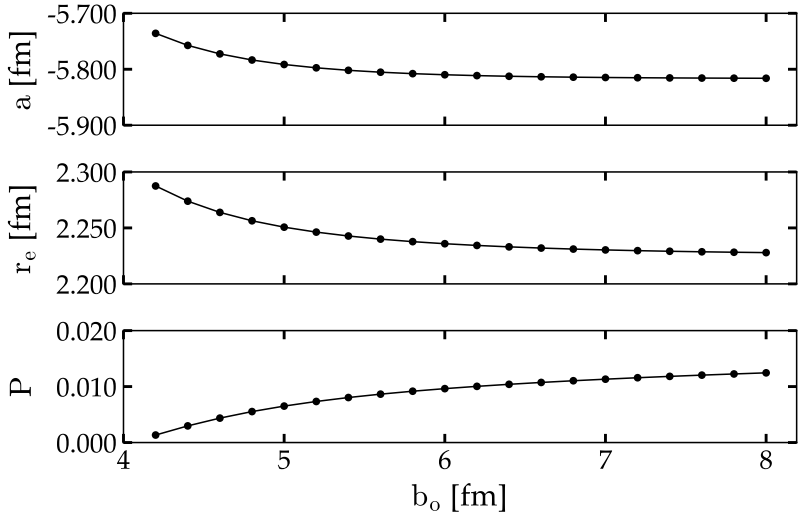


Figure 5.4: Convergence of the scattering parameters for neutron-proton scattering in $\sigma$MEM with respect to $b_o$. The dots represent the parameters calculated from the energies of the preceding two fermi. The solid lines indicate the trend of the convergence.

## 5.2 Neutron-Proton Scattering in $\pi$MEM

Pions are the lightest mesons and thus reside under the smallest potential barrier. It would therefore seem reasonable that any meson exchange model – such as MEM – should include pions. In this section, we include the pion exchange contribution in MEM and calculate the corresponding scattering parameters in the one-pion approximation.

### 5.2.1 One-Pion Approximation

As was the case in $\sigma$MEM, the physical deuteron is a two-component structure in the one-pion approximation

$$\Psi = \begin{pmatrix} \psi_{\text{np}} \\ \psi_{\text{NN}\pi} \end{pmatrix}, \tag{5.21}$$

where $\psi_{\text{np}}$ is the bare deuteron and $\psi_{\text{NN}\pi}$ is the bare deuteron dressed with one pion as indicated by the subscript. Notice that we have named the second entry, $\psi_{\pi\text{NN}}$, in general terms, as the $\pi$-system is actually a superposition of np$\pi^0$, pp$\pi^-$ and nn$\pi^+$ [1].

[1] $$\Psi = \begin{pmatrix} \psi_{\text{np}} \\ \psi_{\text{np}\pi^0} \\ \psi_{\text{nn}\pi^+} \\ \psi_{\text{pp}\pi^-} \end{pmatrix}$$

Assuming that quantities such as isospin, angular momentum and parity are conserved during the nuclear interaction, we can introduce the following pion-nucleon operator[2] [27, 29]

$$W \equiv (\vec{\tau}_1\vec{\pi})(\vec{\sigma}_1\vec{r}_1)F(r_1) + (\vec{\tau}_2\vec{\pi})(\vec{\sigma}_2\vec{r}_2)F(r_2), \tag{5.22}$$

where $\vec{\tau}_i$ and $\vec{\sigma}_i$ are the isovectors of Pauli matrices acting on the i'th nucleon in isospin- and spin space; $\vec{\pi}$ is the isovector of the pions, where $\pi^0$ and $\pi^\pm$ are the physical pions; $\vec{r}_i$ is the relative coordinate between the i'th nucleon and the pion.

Lastly, $F(r_i)$ is a phenomenological short-range formfactor which we can introduce on a Gaussian form

$$F(r_i) = S_w f(r_i)\ \exp\left(-\frac{r_{\text{NN}}^2}{b_{\text{NN}}^2}\right) = S_w A \exp\left(-\frac{r_i^2}{b_w^2}\right)\exp\left(-\frac{r_{\text{NN}}^2}{b_{\text{NN}}^2}\right), \tag{5.23}$$

where $S_w$ is the coupling strength and $A$ is a normalisation constant[3][30]

$$A = \left(4\pi\frac{3\sqrt{\pi}b_w^5}{2^{\frac{11}{2}}}\right).$$

2 The $W^\dagger$-operator includes an integral to remove the coordinates of the annihilated pion.
3 $A$ is chosen such that $\int_{\mathbb{R}^3} d^3r_i r_i^2 f^2(r_i) = 1$

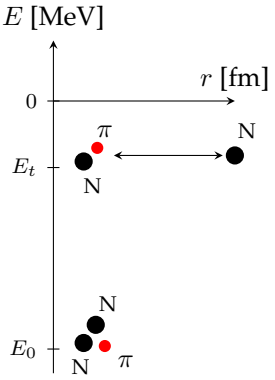


Figure 5.5: Threshold $E_t$ when allowing dressing of individual nucleons.

Consequently, $S_w$ is in units of energy. The short-range formfactor essentially confines the pion to be close to one of the nucleons. We include a factor $\exp\left(-\frac{r_{\mathrm{NN}}^2}{b_{\mathrm{NN}}^2}\right)$ which confines the nucleons in the system to remain close. Otherwise, the $W$-operator would allow for dressing of individual nucleons by pions, thus shifting the system threshold (see Figure 5.5).

We can construct the Hamiltonian matrix acting upon the physical deuteron in the one-pion approximation. In relative Jacobi coordinates it is given as

$$H = \begin{pmatrix} \hat{K}_{\mathrm{d}} + V_{\mathrm{osc}} & W^\dagger \\ W & \hat{K}_\pi + m_\pi \end{pmatrix}. \tag{5.24}$$

By an analogous argument to the $\sigma$MEM we only include the oscillator trap in the bare deuteron system. The Hamiltonian should strictly speaking account for the mass difference between the $\pi^0$ and $\pi^\pm$[31], which are all present in the wave function as discussed above. Similarly, the $\psi_{\pi^-\mathrm{pp}}$-term gives rise to a Coulomb interaction. However, previous work on the one-pion approximation has shown these effects to be negligible [32, 33].

The $W$ in Eq. (5.22) contains operators that act on the nucleon's spin and isospin states. We therefore have to consider the spin and isospin properties of the nucleons. Since nucleons are fermions, the total wave function of the system must be antisymmetric. The deuteron wave function consists primarily of an S = 1, L = 0 state. Thus, it seems reasonable to restrict ourselves to consider s-wave scattering. The spin and spatial parts of the wave function are both symmetric, and so for the total wave function to be antisymmetric, we require the isospin part of the wave function to be antisymmetric. The deuteron, then must be in an isopin singlet state, with $I = 1/2$, $I_3 = \pm 1/2$. The wave function of the bare deuteron can then be written as[4][19, 29]

$$\psi_{\mathrm{np}} = \frac{|\mathrm{pn}\rangle - |\mathrm{np}\rangle}{\sqrt{2}} |\uparrow\uparrow\rangle \sum_{i=1}^{N} c_i \exp\left(\mathbf{r}_{\mathrm{np}}^{\mathsf{T}} A_i \mathbf{r}_{\mathrm{np}}\right). \tag{5.25}$$

The spin-isospin structure of $\psi_{\mathrm{NN}\pi}$,

$$\begin{aligned}\psi_{\pi\mathrm{NN}} = &\left[(\vec{\tau}_1\vec{\pi})(\vec{\sigma}_1\vec{r}_1)+(\vec{\tau}_2\vec{\pi})(\vec{\sigma}_2\vec{r}_2)\right] \\ &\times \frac{|\mathrm{pn}\rangle - |\mathrm{np}\rangle}{\sqrt{2}} |\uparrow\uparrow\rangle \sum_{i=1}^{N} c_i \exp\left(\mathbf{r}_\pi^{\mathsf{T}} A_i \mathbf{r}_\pi\right),\end{aligned} \tag{5.26}$$

4 we define the isospin states of the proton and neutron as $|p\rangle = \begin{pmatrix}1\\0\end{pmatrix}$ and $|n\rangle = \begin{pmatrix}0\\1\end{pmatrix}$

can be inferred by explicitly writing out the Schrödinger equation.

### 5.2.2 Revised Matrix Elements in the One-Pion Approximation

The resultant Hamiltonian and overlap matrices in the one-pion approximation are given as[5]

$$\mathcal{H} = \begin{pmatrix} \langle\psi_i^{\mathrm{d}}|\hat{K}_{\mathrm{d}}|\psi_j^{\mathrm{d}}\rangle & \langle\psi_i^{\mathrm{d}}|W^\dagger|\psi_j^{\pi}\rangle \\ \langle\psi_i^{\pi}|W|\psi_j^{\mathrm{d}}\rangle & \langle\psi_i^{\pi}|\hat{K}_{\pi}+m_\pi|\psi_j^{\pi}\rangle \end{pmatrix}, \qquad \mathcal{N} = \begin{pmatrix} \langle\psi_i^{\mathrm{d}}|\psi_j^{\mathrm{d}}\rangle & 0 \\ 0 & \langle\psi_i^{\pi}|\psi_j^{\pi}\rangle \end{pmatrix}. \tag{5.27}$$

As a consequence of the spin and isospin structure on the wave function, the matrix elements of section 2.4 gain additional front factors.

#### Overlaps

We start by considering the overlaps. The overlap between two $\psi_{\mathrm{d}}$-states is straightforward

$$\begin{aligned} \langle\psi_i^{\mathrm{d}}|\psi_j^{\mathrm{d}}\rangle &= \frac{1}{2}\Big\langle A_i^{\mathrm{d}}\Big| \left(\langle \mathrm{pn}| - \langle \mathrm{np}|\right)\left(|\mathrm{pn}\rangle - |\mathrm{np}\rangle\right)\langle\uparrow\uparrow|\uparrow\uparrow\rangle\Big|A_j^{\mathrm{d}}\Big\rangle && (5.28)\\ &= \langle A_i^{\mathrm{d}}|A_j^{\mathrm{d}}\rangle = M_0, && (5.29)\end{aligned}$$

where we exploit the orthogonality of the spin and isospin states. The picture becomes slightly more complicated for the overlap between $\psi_{np\pi}$-states since the $\vec{\tau}$- and $\vec{\sigma}$-operators act upon the spin- and isospin-states

$$\begin{aligned} \langle\psi_i^{\pi}|\psi_j^{\pi}\rangle = \frac{1}{2}\Big\langle A_i^{\pi}\Big|\langle\uparrow\uparrow|\left[\langle \mathrm{pn}| - \langle \mathrm{np}|\right]\left[(\vec{\tau}_1\vec{\pi})(\vec{\sigma}_1\vec{r}_1) + (\vec{\tau}_2\vec{\pi})(\vec{\sigma}_2\vec{r}_2)\right]^\dagger \\ \times\left[(\vec{\tau}_1\vec{\pi})(\vec{\sigma}_1\vec{r}_1) + (\vec{\tau}_2\vec{\pi})(\vec{\sigma}_2\vec{r}_2)\right]\left[|\mathrm{pn}\rangle - |\mathrm{np}\rangle\right]|\uparrow\uparrow\rangle\Big|A_j^{\pi}\Big\rangle. \end{aligned} \tag{5.30}$$

We start by considering the product of the spin and isospin states, from which we get four terms

$$\begin{aligned} &(\vec{\tau}_1\vec{\pi})^\dagger(\vec{\sigma}_1\vec{r}_1)^\dagger(\vec{\tau}_1\vec{\pi})(\vec{\sigma}_1\vec{r}_1) + (\vec{\tau}_1\vec{\pi})^\dagger(\vec{\sigma}_1\vec{r}_1)^\dagger(\vec{\tau}_2\vec{\pi})(\vec{\sigma}_2\vec{r}_2) \\ &+(\vec{\tau}_2\vec{\pi})^\dagger(\vec{\sigma}_2\vec{r}_2)^\dagger(\vec{\tau}_1\vec{\pi})(\vec{\sigma}_1\vec{r}_2) + (\vec{\tau}_2\vec{\pi})^\dagger(\vec{\sigma}_2\vec{r}_2)^\dagger(\vec{\tau}_2\vec{\pi})(\vec{\sigma}_2\vec{r}_2). \end{aligned} \tag{5.31}$$

The first and last terms are easily calculated using relations for the matrix vectors[6]

$$(\vec{\tau}_1\vec{\pi})^\dagger(\vec{\sigma}_1\vec{r}_1)^\dagger(\vec{\tau}_1\vec{\pi})(\vec{\sigma}_1\vec{r}_1) = 3r_1^2, \tag{5.32}$$

$$(\vec{\tau}_2\vec{\pi})^\dagger(\vec{\sigma}_2\vec{r}_2)^\dagger(\vec{\tau}_2\vec{\pi})(\vec{\sigma}_2\vec{r}_2) = 3r_2^2. \tag{5.33}$$

6 $(\vec{\sigma}\vec{r})^\dagger(\vec{\sigma}\vec{r}) = r^2$ $(\vec{\tau}\vec{\pi})^\dagger(\vec{\tau}\vec{\pi}) = 3.$

5 $|\psi_i^{\mathrm{d}}\rangle$ and $|\psi_i^{\pi}\rangle$ are the transformed wave functions

For the middle two terms, we exploit that $\vec{\sigma}$ and $\vec{\tau}$ act upon the spin and isospin states, respectively. For the second term

$$\langle\uparrow\uparrow|(\vec{\sigma}_1\vec{r}_1)^\dagger(\vec{\sigma}_2\vec{r}_2)|\uparrow\uparrow\rangle = r_1^z r_2^z, \tag{5.34}$$

$$\frac{1}{2}\left[\langle \mathrm{pn}| - \langle \mathrm{np}|\right](\vec{\tau}_1\vec{\pi})^\dagger(\vec{\tau}_2\vec{\pi})\left[|\mathrm{pn}\rangle - |\mathrm{np}\rangle\right] = -3. \tag{5.35}$$

The third term is calculated analogously. The overlap thus becomes

$$\begin{aligned}\langle\psi_i^\pi|\psi_j^\pi\rangle &= \Big\langle A_i^\pi\Big|3r_1^2 - 3r_1^z r_2^z - 3r_1^z r_2^z + 3r_2^2\Big|A_j^\pi\Big\rangle \\ &= 3\Big\langle A_i^\pi\Big|r_1^2 + r_2^2 - 2r_1^z r_2^z\Big|A_j^\pi\Big\rangle.\end{aligned} \tag{5.36}$$

The $\vec{r}_i$- and $w_i$-vectors can now be transformed into relative Jacobi coordinates applying the transformation laws of section 2.5.

$$\mathbf{r}_\pi \to J\mathbf{r} \qquad w_i \to U^\mathsf{T} w_i. \tag{5.37}$$

The relevant $w_i$-vectors are the ones picking out the relative distance between each nucleon and the pion[7]. Since $\mathbf{r} = (\vec{r}_\mathrm{n}, \vec{r}_\mathrm{p}, \vec{r}_\pi)^\mathsf{T}$ then $r_i = w_i^\mathsf{T}\mathbf{r}$. The z-components of the $w_i r_\pi$-vectors are given as

$$r_{\pi i}^z = \vec{e}_z \cdot (w_i^\mathsf{T}\mathbf{r}_\pi) = (\vec{e}_z w_i)^\mathsf{T}\mathbf{r}_\pi. \tag{5.38}$$

Thus, finally, we have in transformed coordinates the following expression for the overlap[8]

$$\begin{aligned}&\langle\psi_i^\pi|\psi_j^\pi\rangle \\ &=3\Big\langle A_i^\pi\Big|(w_1^\mathsf{T}\mathbf{r}_\pi)(w_1^\mathsf{T}\mathbf{r}_\pi) + (w_2^\mathsf{T}\mathbf{r}_\pi)(w_2^\mathsf{T}\mathbf{r}_\pi) - 2(\mathbf{a}^\mathsf{T}\mathbf{r}_\pi^\mathsf{T})(\mathbf{b}^\mathsf{T}\mathbf{r}_\pi)\Big|A_j^\pi\Big\rangle \\ &=\frac{3}{2}\Big\langle A_i^\pi\Big|A_j^\pi\Big\rangle\left[3w_1^\mathsf{T}Rw_1 + 3w_2^\mathsf{T}Rw_2 - 2\mathbf{a}^\mathsf{T}R\mathbf{b}\right] \equiv M_\pi,\end{aligned} \tag{5.39}$$

where we have renamed $(\vec{e}_z w_1) = \mathbf{a}$ and $(\vec{e}_z w_2) = \mathbf{b}$.

7 These are given as

$$w_1 = \begin{pmatrix}1\\0\\-1\end{pmatrix}, \qquad w_2 = \begin{pmatrix}0\\1\\-1\end{pmatrix}$$

8 In the last step, we have carried out the matrix elements exploiting that $\big\langle B\big|(w^\mathsf{T}\mathbf{r})(w^\mathsf{T}\mathbf{r})\big|A\big\rangle = \frac{3}{2}w^\mathsf{T}RwM_0$

**Hamiltonian**

Next, we consider the Hamiltonian matrices. Once again, the first entry on the diagonal is straightforward since we have no operators acting upon the spin and isospin states

$$\begin{aligned}\langle\psi_i^{\mathrm{d}}|\hat{K}_{\mathrm{d}}|\psi_j^{\mathrm{d}}\rangle &= \frac{1}{2}\Big\langle A_i^{\mathrm{d}}\Big|\left(\langle \mathrm{pn}| - \langle \mathrm{np}|\right)\hat{K}_{\mathrm{d}}\left(|\mathrm{pn}\rangle - |\mathrm{np}\rangle\right)\langle\uparrow\uparrow|\uparrow\uparrow\rangle\Big|A_j^{\mathrm{d}}\Big\rangle \\ &= \langle A_i^{\mathrm{d}}|\hat{K}_{\mathrm{d}}|A_j^{\mathrm{d}}\rangle \\ &= 6\mathrm{Tr}\left(BKAR\right)M_0.\end{aligned} \tag{5.40}$$

The matrix element in the $\pi$-system becomes

$$\begin{aligned}&\langle\psi_i^{\pi}|\hat{K}_{\pi}|\psi_j^{\pi}\rangle \\ &\quad= \frac{1}{2}\Big\langle A_i^{\pi}\Big|\langle\uparrow\uparrow|\left[\langle \mathrm{pn}| - \langle \mathrm{np}|\right]\left[(\vec{\tau}_1\vec{\pi})(\vec{\sigma}_1\vec{r}_1) + (\vec{\tau}_2\vec{\pi})(\vec{\sigma}_2\vec{r}_2)\right]^{\dagger} \\ &\quad\times(\hat{K}_{\pi} + m_{\pi})\left[(\vec{\tau}_1\vec{\pi})(\vec{\sigma}_1\vec{r}_1) + (\vec{\tau}_2\vec{\pi})(\vec{\sigma}_2\vec{r}_2)\right]\left[|\mathrm{pn}\rangle - |\mathrm{np}\rangle\right]|\uparrow\uparrow\rangle\Big|A_j^{\pi}\Big\rangle.\end{aligned} \tag{5.41}$$

The calculation resembles that of (5.39), but carrying through an additional factor of $\hat{K}_{\pi}$. Analogous to Eq. (5.36) we get four terms

$$\langle\psi_i^{\pi}|\hat{K}_{\pi}|\psi_j^{\pi}\rangle = \Big\langle A_i^{\pi}\Big|3r_1^2\hat{K}_{\pi} - 3r_1^z\hat{K}_{\pi}r_2^z - 3r_2^z\hat{K}_{\pi}r_1^z + 3r_2^2\hat{K}_{\pi}\Big|A_j^{\pi}\Big\rangle. \tag{5.42}$$

As for the overlap, we transform into Jacobi coordinates. The matrix elements on the form $\langle B, \mathbf{b}|(\mathbf{b}^{\mathsf{T}}\mathbf{r})K(\mathbf{a}^{\mathsf{T}}\mathbf{r})|A, \mathbf{a}\rangle$ can be found in [18]

$$\begin{aligned}\langle\psi_i^{\pi}|\hat{K}_{\pi}|\psi_j^{\pi}\rangle &= 6\mathrm{Tr}\left(BKAR\right)M_{\pi} \\ &\quad+ \left(9w_1^{\mathsf{T}}K'w_1 + 9w_2^{\mathsf{T}}K'w_2 - 3\mathbf{a}^{\mathsf{T}}K'\mathbf{b} - 3\mathbf{b}^{\mathsf{T}}K'\mathbf{a}\right)M_0,\end{aligned} \tag{5.43}$$

where $K' = ((1 - RB)K(1 - AR) + RAKBR)$.

The coupling matrix element resembles the above matrix elements since it carries the same spin-isospin structure

$$\langle\psi_i^{\pi}|W|\psi_j^{\mathrm{d}}\rangle = 3\Big\langle A_i^{\pi}\Big|r_1^2F(r_1) - r_1^zr_2^z\left[F(r_1) + F(r_2)\right] + r_2^2F(r_2)\Big|A_j^{\mathrm{d}}\Big\rangle. \tag{5.44}$$

Carrying out this calculation involves terms such as

$$\begin{aligned}\Big\langle A_i^{\pi}\Big|F(r_l)\Big|A_j^{\mathrm{d}}\Big\rangle &= AS_w\Big\langle A_i^{\pi}\Big|\exp\left(-\frac{r_l^2}{b_w^2}\right)\exp\left(-\frac{r_{\mathrm{NN}}^2}{b_{\mathrm{NN}}^2}\right)\Big|A_j^{\mathrm{d}}\Big\rangle \\ &= AS_w\Big\langle A_i^{\pi}\Big|\tilde{A}_j^l\Big\rangle,\end{aligned} \tag{5.45}$$

where we introduce

$$\tilde{A}_j^l = \begin{pmatrix} A_j^{\mathrm{d}} + \frac{1}{b_{NN}^2} & 0 \\ 0 & 0 \end{pmatrix} + \frac{w_l w_l^{\mathsf{T}}}{b_w^2}. \tag{5.46}$$

The resulting coupling matrix element is thus

$$\begin{aligned} &\langle \psi_i^\pi | W | \psi_j^d \rangle \\ &\qquad = 3AS_w \Bigg[ w_1^{\mathsf{T}} R^1 w_1 \Big\langle A_i^\pi \Big| \tilde{A}_j^1 \Big\rangle - \mathbf{b}^{\mathsf{T}} R^1 \mathbf{a} \Big\langle A_i^\pi \Big| \tilde{A}_j^1 \Big\rangle \\ &\qquad\qquad + \mathbf{a}^{\mathsf{T}} R^2 \mathbf{b} \Big\langle A_i^\pi \Big| \tilde{A}_j^2 \Big\rangle + w_2^{\mathsf{T}} R^2 w_2 \Big\langle A_i^\pi \Big| \tilde{A}_j^2 \Big\rangle \Bigg], \end{aligned} \tag{5.47}$$

where $R^l = (A_i^\pi + \tilde{A}_j^l)$.

### 5.2.3 $\pi$MEM Spectrum

The $\pi$MEM is implemented with parameters $S_w = 75.3$ MeV, $b_w = 1.5$ fm and $b_{NN} = 3.6$ fm, which provide the correct values for the ground state energy $E_0 = -2.22$ MeV and charge radius $R_c = 2.12$ fm for the deuteron [32]. The spectrum of eigenenergies near threshold for the $\pi$MEM can be seen in Figure 5.6. The parameters of the Gaussians we optimised by minimising the sum of the ground and first excited state for $15$ Gaussians in the $np$-subsystem and $50$ Gaussians in the $\pi$-subsystem. Again, the masses of the nucleons were set at $m_p = m_n = 939$ MeV, and the pion mass was set at $m_\pi = 140$ MeV. The extracted scattering parameters in the $\pi$MEM were

$$a = -5.86 \text{ fm}, \qquad r_e = 2.29 \text{ fm}, \qquad P = 0.011.$$

Again, the energies of the ground and first excited state collected from the last two fermi were used in the fit. The parameters are of roughly the same size as was the case for the $\sigma$MEM and thus also overestimate the scattering observables compared to the experimental values. The convergence of the parameters is presented in Figure 5.7.

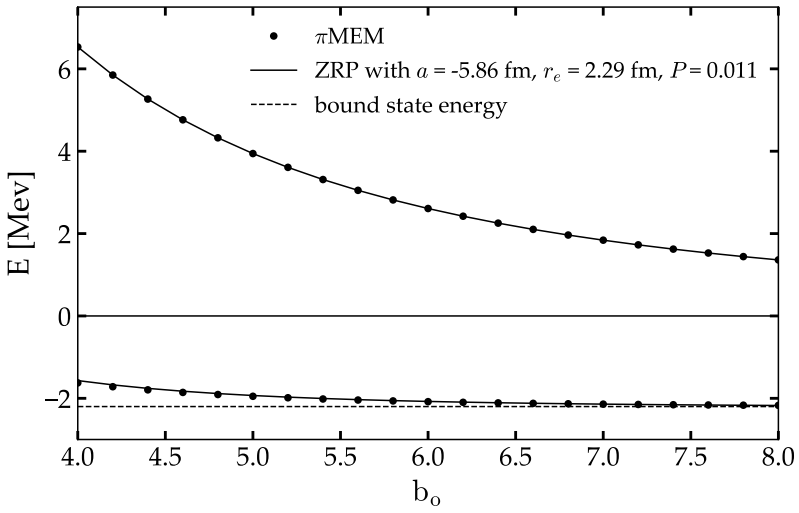


Figure 5.6: The dots show the two lowest eigenenergies of the neutron-proton system in an oscillator trap in $\pi$MEM. The solid lines show the corresponding eigenenergies calculated from Eq. (3.17) with $a = -5.86$ fm, $r_e = 2.29$ fm and $P = 0.011$. The dashed line indicates the bound state energy of the deuteron [32]. The line at zero indicates the threshold.

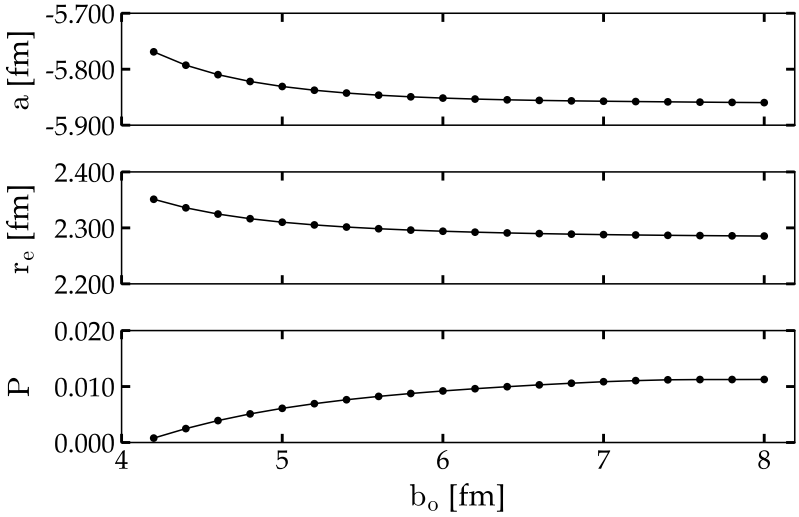


Figure 5.7: Convergence of parameters for low energy neutron-proton scattering in the $\pi$MEM-model with respect to the trap size. Each dot represents a parameter calculated from the preceding two fermi. The solid lines indicate the trend of convergence.

## 5.3 Neutron-Deuteron Scattering in $\sigma$MEM:

As a concluding part of this thesis, we attempt to apply the ACP-recipe to neutron-deuteron scattering in MEM within the one-sigma approximation. In the end, it was not possible to find a realistic set of parameters, $S_\sigma$, and $b_\sigma$, for the model, and we were unable to apply the recipe. Nonetheless, we include our results for future work on the topic.

Some slight adjustments are needed from the deuteron $\sigma$MEM, although the overall ideas remain the same. The wave function is still a two-component structure

$$\Psi = \begin{pmatrix} \psi_{\mathrm{npn'}} \\ \psi_{\mathrm{npn'}\sigma} \end{pmatrix}, \tag{5.48}$$

where $\psi_{pn_1n_2}$ describes the bare triton subsystem and $\psi_{\sigma pn_1n_2}$ the triton-sigma subsystem. The relevant Hamiltonian acting upon (5.48) is a $2 \times 2$ block-matrix

$$H = \begin{pmatrix} \hat{K}_{\mathrm{n}} + \hat{K}_{\mathrm{p}} + \hat{K}_{\mathrm{n'}} + V_{\mathrm{trap}} & W_{\mathrm{np}} + W_{\mathrm{pn'}} + W_{\mathrm{nn'}} \\ W_{\mathrm{np}} + W_{\mathrm{pn'}} + W_{\mathrm{nn'}} & \hat{K}_{\mathrm{n}} + \hat{K}_{\mathrm{p}} + \hat{K}_{\mathrm{n'}} + \hat{K}_\sigma + m_\sigma \end{pmatrix}, \tag{5.49}$$

$W$ are the operators creating and annihilating a sigma meson. Note that three separate coupling operators are needed to describe the creation and annihilation of sigma-mesons between each pair of nucleons in the triton. Each instance of $W$ creates/annihilates a $\sigma$-meson between two nucleons. Each of the coupling operators is defined analogously to (5.10) and (5.11). We should be able to recover the bound state of the deuteron within the triton for the parameters given in [14]. This serves as a sanity check that the model is correctly implemented. This is done by disconnecting the coupling between the nn′ and pn′ nucleon pair. The resulting binding energy can be seen on Figure 5.8.

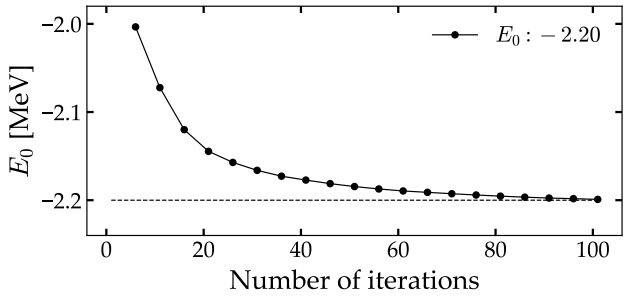


Figure 5.8: Binding energy of the decoupled system as a function of the number of refinement cycles in the optimisation. The oscillator trap was removed from the Hamiltonian.

The system is optimised for the ground state energy with 15 Gaussians in the bare system and 50 Gaussians in the sigma system. The model produces an energy of $-2.2$ MeV. Allowing coupling between all nucleons for the same set of parameters, we find that the triton is overbound at $-97.2$ MeV.

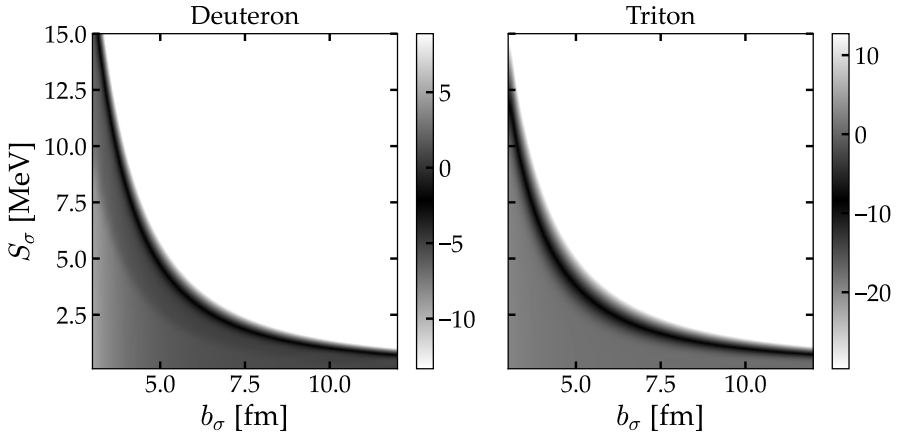


Figure 5.9: The ground state energy of each nucleus as a function of parameters $S_\sigma$ and $b_\sigma$. The black areas show the combination of parameters corresponding to the correct binding energies for the deuteron and triton, respectively.

To find a pair of parameters that can produce the correct binding energy for the deuteron and the triton, we search through the parameter space. We vary the strength and range parameter independently, to see which set of parameters produces the correct binding energies. This is illustrated in Figure 5.9. The model must bind the triton and the deuteron states simultaneously for a realistic single set of parameters. This corresponds to the intersection point in Figure 5.10.

The parameters at the intersection are

$$S_\sigma = 0.771 \text{ MeV}, \qquad b_\sigma = 10.57 \text{ fm}.$$

A $b_\sigma$ value of $10.57$ fm is well outside the scope of what might be considered realistic. $b_\sigma$ should be approximately around the size of the deuteron, that is, in the range of around 2-3 fm.

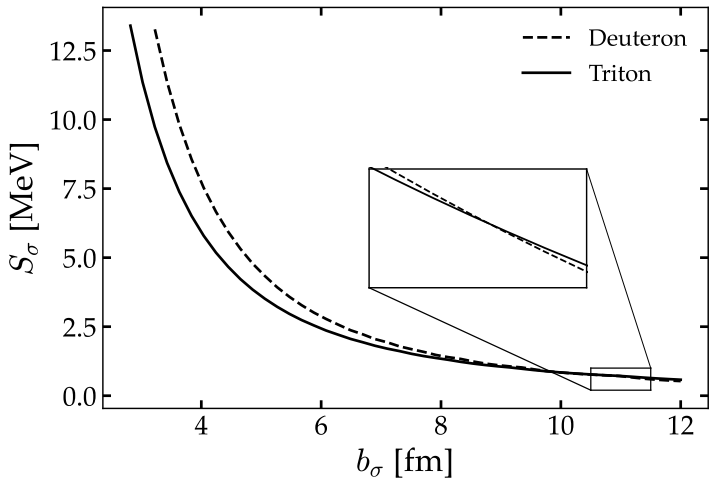


Figure 5.10: Interpolation of combinations of parameters corresponding to the correct binding energies from Figure 5.9. The intersection point yields a set of parameters that can bind both nuclei simultaneously. The intersection point is highlighted in the zoomed graph.

# CHAPTER 6

# Discussion

The initial test of the recipe, considering a deuteron in a Volkov potential, was very promising. The extracted value for the scattering length very closely matches the value reported in [26], and the zero-range formula accurately reproduced the spectrum near threshold for the corresponding parameters.

The best results for this system were obtained for a combination of the ground and 1st excited state. This makes sense as we expect inclusion of additional states to improve the fidelity of the fit, provided that these are within the limits of the effective range approximation[1]. In this case, the weakly bound ground state ($E_0 = 0.546$ MeV) and 1st excited state both fall well within this domain.

An attempt was made to include higher energy levels; however, even including just the 2nd excited level, the model parameters did not converge as well as the combination of the ground and 1st excited states. The energies of the 2nd excited state may not be sufficiently converged, requiring more Gaussians for the higher lying states to be included. Alternatively, it may be that the 2nd excited state is outside the scope of the effective range formula, demanding a larger $b_0$ for convergence.

The triton in a Volkov potential presented significant challenges. The zero-range formula could only reproduce the part of the spectrum to which it was fitted, and thus there was some limitation to its applicability for this system. Convergence was achieved for the scattering length and effective range when fitting the 1st excited state. The shape

1 Recall that this is a Taylor expansion at $E \to 0$

parameter did not appear to converge, as evident from figure 4.9, perhaps indicating that the 3rd order expansion is not overly important for the model. However, as argued in section 4.1.1, inclusion of the shape parameter seemed to improve the convergence for the scattering length and, in particular, the effective range.

Including the ground state in the fit resulted in more or less the same parameters as fitting the 1st excited state alone, with the corresponding parameters reasonably converged. This is somewhat unintuitive as we would expect the ground state energy, $E_0 = -8.431$ MeV, to be outside the valid range of the effective range formula, and thus too far from threshold to be considered in the fit. Perhaps a more indepth analysis of the valid range of the effective range approximation could potentially help clarify whether this is the case.

We would expect a combination of higher-lying states to give better results. However, convergence could not be accomplished for combinations including the 2nd excited state. The energies at large $b_\mathrm{o}$'s are close to the threshold of the system, and are thus within the range of the zero-range approximation. The straightforward explanation might simply be that the energies themselves were not properly converged. The system was optimised for 200 Gaussians in total, which proved computationally demanding. Due to time constraints, further refinement of the energies was not pursued. Perhaps future work on this system would benefit from considering more intricate optimisation strategies than those employed in this investigation.

Arguably, the choice of threshold is critical to ensure convergence of the scattering variables. In the end, convergence could only be achieved when setting the threshold value at the final energy of 1st excited level. Our search for an optimal threshold resulted in a value, slightly above the 1st excited level, which was somewhat unexpected, as this level defines the threshold. However, the effect of the optimal threshold value upon the scattering parameters was not very substantial in any case.

As for the deuteron in the Volkov potential, the zero-range model fits the data very well for the $\sigma$- and $\pi$MEM. Both models give roughly the same scattering length within around $1\%$. This is not unexpected as both models are parametrised to give the same value for the ground state and charge radius. The affiliated parameters are model independent under the effective range approximation and should therefore produce

the same parameters. The small discrepancies can likely be explained by slight inaccuracies in the tuning of the model parameters.

Even so, it is clear that neither model suffice to describe nucleon-nucleon scattering. This is not unexpected as we restricted ourselves to simple one-meson approximations in both cases. Both models suppress the dressing of individual nucleons in the deuteron. One could make the pion model more realistic by removing this restriction, letting $b_{NN}$ become large and investigate the corresponding spectrum. The threshold of the system would shift to the binding energy of the dressed nucleon in this case. Its clear that the contribution from D-waves should also be considered, as experiments show that the deuteron has a quadrupole moment which is induced by the D-wave contribution. However, D-waves only contribute around $4\%$ of the total wave function for the deuteron [29]. One would have to carry through the calculations to estimate the effect of these contributions.

Only one set of parameters could bind the triton and deuteron simultaneously in the $\sigma$MEM, namely $S_\sigma = 0.771$ MeV and $b_\sigma = 10.57$ fm. However, the acquired range parameter was far outside of what might be considered realistic for $b_\sigma$. Possibly the reason a large value of $b_\sigma$ is needed to bind the triton and deuteron simultaneously is that small $b_\sigma$'s suppress the states where the incoming neutron and the deuteron are far apart in (5.11). Thus, we did not attempt to subject the model to our ACP recipe.

# Chapter 7

# Conclusion

This thesis introduces a new ACP type recipe for the calculation of low-energy scattering parameters – scattering length, effective range and first shape parameter – relying exclusively on discrete spectrum calculations. The few-body system is placed in an appropriately sized oscillator trap, turning the continuum into a quasi-continuum. The recipe explicitly targets the low-energy scattering parameters, which are extracted from the discrete energy spectrum through its functional dependence upon the trap size. These are related through an analytic formula which can be fitted to the spectrum near threshold.

The recipe was first validated using a Volkov potential. Results for the deuteron were very promising; however, there were clearly challenges concerning the triton system, as the zero-range formula could not reproduce the full spectrum. While these issues may stem from numerical imprecision in the calculated spectrum, we cannot decisively rule out inherent limitations in the recipe itself. It seems like further investigation is needed on this system.

Having validated the recipe for NN scattering, it was then applied to the deuteron in MEM. Results for the MEM models overestimated the scattering parameters by roughly 10-20%. While these can be considered qualitatively correct, this suggests that neither the one-sigma nor the one-pion approximation are sufficient to describe NN scattering.

No realistic pair of single parameters could bind the triton and deuteron simultaneously in the one-sigma approximation, and the model was consequently not subjected to the ACP recipe. Arguably the one-sigma approximation was too much of a simplification.

# Bibliography


[1] Jim Mitroy et al. 'Theory and application of explicitly correlated Gaussians'. In: *Rev. Mod. Phys.* 85 (2 May 2013), pp. 693–749.

[2] J. Y. Zhang, J. Mitroy and K. Varga. 'Development of a confined variational method for elastic scattering'. In: *Phys. Rev. A* 78 (4 Oct. 2008), p. 042705.

[3] J. Mitroy, J. Y. Zhang and K. Varga. 'Elastic Scattering Using an Artificial Confining Potential'. In: *Phys. Rev. Lett.* 101 (12 Sept. 2008), p. 123201.

[4] R Guérout, M Jungen and Ch Jungen. 'Ab initio molecular quantum defect theory: I. Method of artificial well potentials'. In: *Journal of Physics B: Atomic, Molecular and Optical Physics* 37.15 (July 2004), p. 3043.

[5] Xilin Zhang. 'Extracting free-space observables from trapped interacting clusters'. In: *Phys. Rev. C* 101 (5 May 2020), p. 051602.

[6] Xilin Zhang et al. 'Ab Initio Calculations of Low-Energy Nuclear Scattering Using Confining Potential Traps'. In: *Physical Review Letters* 125.11 (Sept. 2020).

[7] Thomas Luu et al. 'Nucleon-nucleon scattering in a harmonic potential'. In: *Phys. Rev. C* 82 (3 Sept. 2010), p. 034003.

[8] Thomas Busch et al. 'Two Cold Atoms in a Harmonic Trap'. In: *Foundations of Physics* 28 (Apr. 1998).

[9] Akira Suzuki, Yi Liang and Rajat K. Bhaduri. 'Two-atom energy spectrum in a harmonic trap near a Feshbach resonance at higher partial waves'. In: *Phys. Rev. A* 80 (3 Sept. 2009), p. 033601.

[10] S.-K. Yip. 'Energy levels of two identical fermions in a harmonic trap near a $p$-wave Feshbach resonance'. In: *Phys. Rev. A* 78 (1 July 2008), p. 013612.

[11] D. V. Fedorov and A. M. Pedersen. 'Calculation of low-energy scattering parameters using artificial oscillator trap'. In: (2025).

[12] D. V. Fedorov. 'Analytic Matrix Elements and Gradients with Shifted Correlated Gaussians'. In: *Few-Body Systems* 58.1 (Dec. 2016).

[13] Y. Suzuki and K. Varga. *Stochastic Variational Approach to Quantum-Mechanical Few-Body problems*. First Edition. Springer-Verlag Berlin Heidelberg 1998, 1998.

[14] D. Fedorov. 'A Nuclear Model with Explicit Mesons'. In: *Few-Body Systems* 61 (Dec. 2020).

[15] Eric Jones, Travis Oliphant, Pearu Peterson et al. *scipy.linalg.eigh — SciPy v1.13.1 Manual*. 2002–.

[16] D. V. Fedorov. 'Correlated Gaussians and Low-Discrepancy Sequences'. In: *Few-Body Systems* 60.3 (July 2019).

[17] J. A. Nelder and R. Mead. 'A Simplex Method for Function Minimization'. In: *The Computer Journal* 7.4 (Jan. 1965), pp. 308–313.

[18] D. V. Fedorov et al. *Explicitly correlated Gaussians with tensor prefactors: analytic matrix elements*. 2024.

[19] J.J. Sakurai and J. Napolitano. *Modern Quantum Mechanics*. Cambridge University Press, 2020.

[20] Melvin Alexander Preston. *Physics of the Nucleus*. Addison-Wesley series in physics. Reading, Mass.: Addison-Wesley Publishing Company, 1962.

[21] Eliton Popovicz Seidel and Felipe Arretche. 'Zero range potential approximation in quantum scattering problems'. In: *American Journal of Physics* 87.10 (Oct. 2019), pp. 796–801.

[22] Lars Madsen. 'Effective range theory'. In: *American Journal of Physics - AMER J PHYS* 70 (Aug. 2002).

[23] H P Noyes. 'The Nucleon-Nucleon Effective Range Expansion Parameters'. In: *Annual Review of Nuclear and Particle Science* 22.Volume 22, 1972 (1972), pp. 465–484.

[24] H. Weber. 'Ueber die Integration der partiellen Differentialgleichung:' in: *Mathematische Annalen* 1 (1869), pp. 1–36.

[25] William J. Thompson. *Atlas for Computing Mathematical Functions: An Illustrated Guide for Practitioners with Programs in FORTRAN*

*and Mathematica with Cdrom*. 1st. USA: John Wiley & Sons, Inc., 1997.

[26] M. Gattobigio and A. Kievsky. 'Universality and scaling in the $N$-body sector of Efimov physics'. In: *Phys. Rev. A* 90 (1 July 2014), p. 012502.

[27] D. V. Fedorov and M. Mikkelsen. 'Threshold Photoproduction of Neutral Pions Off Protons in Nuclear Model with Explicit Mesons'. In: *Few-Body Systems* 64.1 (Dec. 2022).

[28] R. W. Hackenburg. 'Neutron-proton effective range parameters and zero-energy shape dependence'. In: *Phys. Rev. C* 73 (4 Apr. 2006), p. 044002.

[29] P. J. Siemens and A. S. Jensen. *Elements of Nuclei: Many-body Physics With The String Interaction*. First Edition. CRC Press, 1987.

[30] D. V. Fedorov. *The N(1440) Roper resonance in the nuclear model with explicit mesons*. 2024.

[31] S. Navas et al. 'Review of Particle Physics'. In: *Phys. Rev. D* 110 (3 Aug. 2024), p. 030001.

[32] Tobias L. Norbohm. 'Deuteron with D-waves in the nuclear model with explicit mesons'. MA thesis. Aarhus University, 2024.

[33] Martin Mikkelsen. 'Threshold Pion Photoproduction off Nucleons using the Nuclear Model with Explicit Pions'. MA thesis. Aarhus University, 2022.

APPENDIX A

# Derivation of Matrix Elements

In this appendix, we go through an in-depth derivation of the matrix elements presented in section 2.4. First, we introduce the following identities, which will come in handy throughout our calculations

$$\partial_{\mathbf{r}}\mathbf{r} = 3N \tag{A.1}$$

$$\partial_{\mathbf{r}}\mathbf{a}^{\mathsf{T}}A\mathbf{r} = \mathbf{a}^{\mathsf{T}}A \tag{A.2}$$

$$\partial_{\mathbf{r}}M\mathbf{r} = 3\mathrm{Tr}(M) \tag{A.3}$$

$$\partial_{\mathbf{r}}\mathbf{r}^{T}M\mathbf{r} = 2\mathbf{r}^{T}M \tag{A.4}$$

These identities are easily proven by direct calculations.

## Overlap Matrix Element:

The most fundamental matrix element is the standard overlap between two Gaussians. Let $|A, \mathbf{a}\rangle$ and $|B, \mathbf{b}\rangle$ be two shifted ECG's with shift vectos **a** and **b** respectively. The standard overlap between them is thus given through the integral

$$\begin{aligned}
\langle B, \mathbf{b}|A, \mathbf{a}\rangle &= \int d\vec{r}_1^{\,3}, \ldots, d\vec{r}_N^{\,3} \langle B, \mathbf{b}|\mathbf{r}\rangle\langle\mathbf{r}|A, \mathbf{a}\rangle \\
&= \int d\vec{r}_1^{\,3}, \ldots, d\vec{r}_N^{\,3} \exp\left(-\mathbf{r}^{\mathsf{T}}B\mathbf{r} + \mathbf{b}^{\mathsf{T}}\mathbf{r}\right) \exp\left(-\mathbf{r}^{\mathsf{T}}A\mathbf{r} + \mathbf{a}^{\mathsf{T}}\mathbf{r}\right) \\
&= \int d\vec{r}_1^{\,3}, \ldots, d\vec{r}_N^{\,3} \exp\left(-\mathbf{r}^{\mathsf{T}}(A+B)\mathbf{r} + (\mathbf{b}+\mathbf{a})^{\mathsf{T}}\mathbf{r}\right) \\
&= \int d\vec{r}_1^{\,3}, \ldots, d\vec{r}_N^{\,3} \exp\left(-\mathbf{r}^{\mathsf{T}}(A+B)\mathbf{r} + \mathbf{v}^{\mathsf{T}}\mathbf{r}\right)
\end{aligned} \tag{A.5}$$

where we have introduced $\mathbf{v} \equiv \mathbf{a} + \mathbf{b}$. As the matrices $A$ and $B$ are both symmetric, the sum is likewise symmetric. The matrix $(A + B)$ is thus self-adjoint, and from the spectral theorem, it follows that there exists an orthonormal basis in which $(A + B)$ is diagonalizable. Thus, we have $(A + B) = Q^{\mathsf{T}} D Q$ for a diagonal matrix $D$ and orthogonal matrix $Q$ for which $Q^{\mathsf{T}} Q = Q Q^{\mathsf{T}} = 1$ [12]. Performing said transformation

$$\begin{aligned}
\langle B, \mathbf{b} | A, \mathbf{a} \rangle &= \int d\vec{x}_1^3, \ldots, d\vec{x}_N^3 \exp\left( -(Q\mathbf{x})^{\mathsf{T}} (A + B) Q\mathbf{x} + \mathbf{v}^{\mathsf{T}} Q\mathbf{x} \right) \\
&= \int d\vec{x}_1^3, \ldots, d\vec{x}_N^3 \exp\left( -\mathbf{x}^{\mathsf{T}} Q^{\mathsf{T}} (A + B) Q\mathbf{x} + \mathbf{v}^{\mathsf{T}} Q\mathbf{x} \right) \\
&= \int d\vec{x}_1^3, \ldots, d\vec{x}_N^3 \exp\left( -\mathbf{x}^{\mathsf{T}} D\mathbf{x} + \mathbf{v}^{\mathsf{T}} Q\mathbf{x} \right)
\end{aligned} \tag{A.6}$$

where $\mathbf{r} = Q\mathbf{x}$. By expanding the exponent and taking $\tilde{\mathbf{v}} = Q^{\mathsf{T}}\mathbf{v}$ for convenience

$$\begin{aligned}
&= \int d\vec{x}_1^3, \ldots, d\vec{x}_N^3 \exp\left( -\sum_{i=1}^{N} D_{ii} \vec{x}_i \vec{x}_i + \sum_{i=1}^{N} \vec{\tilde{v}}_i \vec{x}_i \right) \\
&= \prod_{i=1}^{N} \int d\vec{x}_i^3 \exp\left( -D_{ii} \vec{x}_i \vec{x}_i + \vec{\tilde{v}}_i \vec{x}_i \right) \\
&= \prod_{i=1}^{N} \int d\vec{x}_i^3 \exp\left( \sum_{k=1}^{3} \left[ -D_{ii} (\vec{x}_i)_k^2 + (\vec{\tilde{v}}_i)_k (\vec{x}_i)_k \right] \right) \\
&= \prod_{i=1}^{N} \int d\vec{x}_i^3 \prod_{k=1}^{3} \exp\left( -D_{ii} (\vec{x}_i)_k^2 + (\vec{\tilde{v}}_i)_k (\vec{x}_i)_k \right) \\
&= \prod_{i=1}^{N} \int d\vec{x}_i^3 \prod_{k=1}^{3} \exp\left( -D_{ii} \left[ (\vec{x}_i)_k^2 - \frac{(\vec{\tilde{v}}_i)_k}{2D_{ii}} \right]^2 + \frac{(\vec{\tilde{v}}_i)_k^2}{4D_{ii}} \right),
\end{aligned} \tag{A.7}$$

where in the final line we have completed the square. (A.7) can be rewritten as

$$= \prod_{i=1}^{N} \exp\left( \frac{\vec{\tilde{v}}_i \cdot \vec{\tilde{v}}_i}{4D_{ii}} \right) \prod_{k=1}^{3} \int d\vec{x}_i^3 \exp\left( -D_{ii} \left[ (\vec{x}_i)_k^2 - \frac{(\vec{\tilde{v}}_i)_k}{2D_{ii}} \right]^2 \right)$$

Calculating the integral we get the final result for the overlap[1]

$$\begin{aligned}\langle A, \mathbf{a}|B, \mathbf{b}\rangle &= \prod_{i=1}^{N} \exp\left(\frac{\vec{v}_i \cdot \vec{v}_i}{4D_{ii}}\right) \prod_{k=1}^{3} \left(\frac{\pi}{D_{ii}}\right)^{\frac{1}{2}} \\ &= \exp\left(\frac{1}{4}\tilde{\mathbf{v}}^{\mathsf{T}} D^{-1} \tilde{\mathbf{v}}\right) \left(\frac{\pi^N}{D}\right)^{\frac{3}{2}} \\ &= \exp\left(\frac{1}{4}\mathbf{v}^{\mathsf{T}} R \mathbf{v}\right) \left(\frac{\pi^N}{(A+B)}\right)^{\frac{3}{2}} \equiv M,\end{aligned}$$

where we have use the fact that $D^{-1}$ is diagonal. We have also introduced $R = (A+B)^{-1}$ For **s**-waves we simply let

$$\langle A|B\rangle \overset{\mathbf{v}\to 0}{=} \left(\frac{\pi^N}{\det(A+B)}\right)^{\frac{3}{2}} \equiv M_0, \tag{A.8}$$

As we shall see, the overlap matrix element turns out to be fundamental to all the remaining matrix elements needed for our investigations.

## Kinetic Energy Matrix Element

We shall use the kinetic energy operator on the form

$$\hat{K} = -\frac{\partial}{\partial \mathbf{r}} K \frac{\partial}{\partial \mathbf{r}^T} = -\partial_{\mathbf{r}} K \partial_{\mathbf{r}^{\mathsf{T}}}, \tag{A.9}$$

where we have introduced the notation $\frac{\partial}{\partial \mathbf{r}} = \partial_{\mathbf{r}}$ in the interest of clarity. $K$ is an $N \times N$ matrix independent of $\mathbf{r}$. We begin by showing that

$$\langle B, \mathbf{b}| - \partial_{\mathbf{r}} K \partial_{\mathbf{r}^{\mathsf{T}}}|A, \mathbf{a}\rangle = \langle \partial_{\mathbf{r}} B, \mathbf{b}|K|\partial_{\mathbf{r}^{\mathsf{T}}} A, \mathbf{a}\rangle. \tag{A.10}$$

We start from the left-hand side of (A.10).

$$\begin{aligned}&\langle B, \mathbf{b}| - \partial_{\mathbf{r}} K \partial_{\mathbf{r}^{\mathsf{T}}}|A, \mathbf{a}\rangle \\ &\quad = -\int_{\mathbb{R}^3} d^3\mathbf{r}_1, d^3\mathbf{r}_2, ..., d^3\mathbf{r}_N \exp\left(-\mathbf{r}^{\mathsf{T}} B \mathbf{r} + \mathbf{b}^{\mathsf{T}} \mathbf{r}\right) \\ &\qquad\qquad \times \partial_{\mathbf{r}} K \partial_{\mathbf{r}^{\mathsf{T}}} \exp\left(-\mathbf{r}^{\mathsf{T}} A \mathbf{r} + \mathbf{a}^{\mathsf{T}} \mathbf{r}\right).\end{aligned} \tag{A.11}$$

1 The last step follows from $\tilde{\mathbf{v}}^{\mathsf{T}} D^{-1} \tilde{\mathbf{v}} = \mathbf{v}^{\mathsf{T}} Q Q^{\mathsf{T}} R Q Q^{\mathsf{T}} \mathbf{v} = \mathbf{v}^{\mathsf{T}} R \mathbf{v}$.

We expand the kinetic operator in component form

$$= -\sum_{i,j=1}^{N} K_{ij} \sum_{m=1}^{3} \int_{\mathbb{R}^3} d^3\mathbf{r}_1, d^3\mathbf{r}_2, ..., d^3\mathbf{r}_N \times \exp\left(-\mathbf{r}^\mathsf{T} B\mathbf{r} + \mathbf{b}^\mathsf{T}\mathbf{r}\right) \left(\partial_{\vec{r}_i}\right)_m \left(\partial_{\vec{r}_j}\right)_m \exp\left(-\mathbf{r}^\mathsf{T} A\mathbf{r} + \mathbf{a}^\mathsf{T}\mathbf{r}\right), \tag{A.12}$$

By notion of the product rule

$$\begin{aligned} &\left(\partial_{\vec{r}_i}\right)_m [f(\mathbf{r})g(\mathbf{r})] = \left(\partial_{\vec{r}_i}\right)_m f(\mathbf{r})g(\mathbf{r}) + f(\mathbf{r}) \left(\partial_{\vec{r}_i}\right)_m g(\mathbf{r}) \\ &\Downarrow \\ &f(\mathbf{r}) \left(\partial_{\vec{r}_i}\right)_m g(\mathbf{r}) = \left(\partial_{\vec{r}_i}\right)_m [f(\mathbf{r})g(\mathbf{r})] - \left(\partial_{\vec{r}_i}\right)_m f(\mathbf{r})g(\mathbf{r}), \end{aligned} \tag{A.13}$$

where $f(\mathbf{r}) = e^{-\mathbf{r}^\mathsf{T} B\mathbf{r} - \mathbf{b}'^\mathsf{T}\mathbf{r}}$ and $g(\mathbf{r}) = \left(\partial_{\vec{r}_j}\right)_m e^{-\mathbf{r}^\mathsf{T} A\mathbf{r} - \mathbf{a}^\mathsf{T}\mathbf{r}}$. Applying this to (A.12) yields two terms. The term

$$-\sum_{i,j=1}^{N} K_{ij} \sum_{m=1}^{3} \int_{\mathbb{R}^{3N}} d^3\mathbf{r}_1, d^3\mathbf{r}_2, ..., d^3\mathbf{r}_N \times \left(\partial_{\vec{r}_i}\right)_m \left[\exp\left(-\mathbf{r}^\mathsf{T} B\mathbf{r} + \mathbf{b}^\mathsf{T}\mathbf{r}\right) \left(\partial_{\vec{r}_j}\right)_m \exp\left(-\mathbf{r}^\mathsf{T} A\mathbf{r} + \mathbf{a}^\mathsf{T}\mathbf{r}\right)\right], \tag{A.14}$$

is 0[2]. We consider now the second term

$$\sum_{i,j=1}^{N} K_{ij} \sum_{m=1}^{3} \int_{\mathbb{R}^3} d^3\mathbf{r}_1, d^3\mathbf{r}_2, ..., d^3\mathbf{r}_N \times \left[\left(\partial_{\vec{r}_i}\right)_m \exp\left(-\mathbf{r}^\mathsf{T} B\mathbf{r} + \mathbf{b}^T\mathbf{r}\right)\right] \left[\left(\partial_{\vec{r}_j}\right)_m \exp\left(-\mathbf{r}^\mathsf{T} A\mathbf{r} + \mathbf{a}^\mathsf{T}\mathbf{r}\right)\right] \tag{A.15}$$

$$= \int_{\mathbb{R}^3} d^3\mathbf{r}_1, d^3\mathbf{r}_2, ..., d^3\mathbf{r}_N \times \left[\partial_{\mathbf{r}} \exp\left(-\mathbf{r}^\mathsf{T} B\mathbf{r} + \mathbf{b}^\mathsf{T}\mathbf{r}\right)\right] K \left[\partial_{\mathbf{r}^\mathsf{T}} \exp\left(-\mathbf{r}^\mathsf{T} A\mathbf{r} + \mathbf{a}^\mathsf{T}\mathbf{r}\right)\right], \tag{A.16}$$

which is the desired identity

$$\langle \partial_{\mathbf{r}} B, \mathbf{b} | K | \partial_{\mathbf{r}^\mathsf{T}} A, \mathbf{a} \rangle. \tag{A.17}$$

2 This can be shown by performing the $(\mathbf{r}_i)_m$'th integral and then exploiting that the Gaussians vanish exponentially in the limits $\pm\infty$

We are now in a position to calculate the kinetic matrix element. We start by employing the result we have just derived

$$\langle B, \mathbf{b}|\hat{K}|A, \mathbf{a}\rangle = \langle B, \mathbf{b}| - \partial_{\mathbf{r}} K \partial_{\mathbf{r}^\mathsf{T}}|A, \mathbf{a}\rangle = \langle \partial_{\mathbf{r}} B, \mathbf{b}|K|\partial_{\mathbf{r}^\mathsf{T}} A, \mathbf{a}\rangle. \quad \text{(A.18)}$$

We can evaluate the derivative by applying identities

$$\begin{aligned} \partial_{\mathbf{r}} \exp\left(-\mathbf{r}^\mathsf{T} B\mathbf{r} + \mathbf{b}^\mathsf{T}\mathbf{r}\right) &= (\mathbf{b} - 2B\mathbf{r})^\mathsf{T} \exp\left(-\mathbf{r}^\mathsf{T} B\mathbf{r} + \mathbf{b}^\mathsf{T}\mathbf{r}\right), \\ \partial_{\mathbf{r}^\mathsf{T}} \exp\left(-\mathbf{r}^\mathsf{T} A\mathbf{r} + \mathbf{a}^\mathsf{T}\mathbf{r}\right) &= (\mathbf{a} - 2A\mathbf{r}) \exp\left(-\mathbf{r}^\mathsf{T} A\mathbf{r} + \mathbf{a}^\mathsf{T}\mathbf{r}\right), \end{aligned} \quad \text{(A.19)}$$

resulting in a matrix element on the form

$$= \langle B, \mathbf{b}|(\mathbf{b} - 2B\mathbf{r})^T K(\mathbf{a} - 2A\mathbf{r})|A, \mathbf{a}\rangle \quad \text{(A.20)}$$

yielding four terms

$$\begin{aligned} &= \mathbf{b}^\mathsf{T} K\mathbf{a}\langle B, \mathbf{b}|A, \mathbf{a}\rangle - 2\mathbf{b}^\mathsf{T} KA\langle B, \mathbf{b}|\mathbf{r}|A, \mathbf{a}\rangle \\ &\quad - 2B^\mathsf{T} K\mathbf{a}\langle B, \mathbf{b}|\mathbf{r}^\mathsf{T}|A, \mathbf{a}\rangle + 4\langle B, \mathbf{b}|\mathbf{r}^\mathsf{T} B^\mathsf{T} KA\mathbf{r}|A, \mathbf{a}\rangle. \end{aligned} \quad \text{(A.21)}$$

We need to evaluate matrix elements in the last three terms. starting with the middle two terms we can substitute the **r**-vector by an appropriate derivative[3]

$$\langle B, \mathbf{b}|\mathbf{r}|A, \mathbf{a}\rangle = \partial_{\mathbf{v}^\mathsf{T}} \langle B, \mathbf{b}|A, \mathbf{a}\rangle \quad \text{(A.22)}$$

where we recall that $R = A + B$ and $\mathbf{v} = \mathbf{b} + \mathbf{a}$.

Recall that $\langle B, \mathbf{b}|A\mathbf{a}\rangle = \exp\left(\frac{1}{4}\mathbf{v}^\mathsf{T} R\mathbf{v}\right) M_0$, where $M_0 = \left(\frac{\pi^N}{\det(A+B)}\right)^{\frac{3}{2}}$. Thus

$$\begin{aligned} \partial_{\mathbf{v}^\mathsf{T}} \langle B, \mathbf{b}|A, \mathbf{a}\rangle &= \partial_{\mathbf{v}^\mathsf{T}} \exp\left(\frac{1}{4}\mathbf{v}^\mathsf{T} R\mathbf{v}\right) M_0 \\ &= \frac{1}{2} R\mathbf{v}\langle B, \mathbf{b}|A, \mathbf{a}\rangle, \end{aligned} \quad \text{(A.23)}$$

3 The inner product is expanded in position space

$$\begin{aligned} \langle B, \mathbf{b}|\mathbf{r}|A, \mathbf{a}\rangle &= \int_{\mathbb{R}^3} d^3\mathbf{r}_1, d^3\mathbf{r}_2, ..., d^3\mathbf{r}_N \exp\left(-\mathbf{r}^\mathsf{T} B\mathbf{r} + \mathbf{b}^\mathsf{T}\mathbf{r}\right) \mathbf{r} \exp\left(-\mathbf{r}^\mathsf{T} A\mathbf{r} + \mathbf{a}^\mathsf{T}\mathbf{r}\right) \\ &= \int_{\mathbb{R}^3} d^3\mathbf{r}_1, d^3\mathbf{r}_2, ..., d^3\mathbf{r}_N \mathbf{r} \exp\left(-\mathbf{r}^\mathsf{T} R\mathbf{r} + \mathbf{v}^\mathsf{T}\right) \\ &= \partial_{\mathbf{v}^\mathsf{T}} \int_{\mathbb{R}^3} d^3\mathbf{r}_1, d^3\mathbf{r}_2, ..., d^3\mathbf{r}_N \exp\left(-\mathbf{r}^\mathsf{T} R\mathbf{r} + \mathbf{v}^\mathsf{T}\right) = \partial_{\mathbf{v}^\mathsf{T}} \langle B, \mathbf{b}|A, \mathbf{a}\rangle \end{aligned}$$

where we have used identity (A.4). The $\langle B, \mathbf{b}|\mathbf{r}^\mathsf{T}|A, \mathbf{a}\rangle$ term is calculated analogously using that $\partial_\mathbf{v} \exp\left(\frac{1}{4}\mathbf{v}^\mathsf{T} R\mathbf{v}\right) = \frac{1}{2}\mathbf{v}^\mathsf{T} R$.

The final term in (A.21) is calculated through a similar approach

$$\begin{aligned}
&\langle B, \mathbf{b}|\mathbf{r}^\mathsf{T} B^\mathsf{T} K A\mathbf{r}|A, \mathbf{a}\\
&\qquad = \int_{\mathbb{R}^3} d^3\mathbf{r}_1, d^3\mathbf{r}_2, ..., d^3\mathbf{r}_N \mathbf{r}^\mathsf{T} B^\mathsf{T} K A\mathbf{r} \exp\left(-\mathbf{r}^\mathsf{T} R\mathbf{r} + \mathbf{a}^\mathsf{T}\mathbf{v}\right)\\
&\qquad = \int_{\mathbb{R}^3} d^3\mathbf{r}_1, d^3\mathbf{r}_2, ..., d^3\mathbf{r}_N \partial_\mathbf{v} B^\mathsf{T} K A \partial_{\mathbf{v}^\mathsf{T}} \exp\left(-\mathbf{r}^\mathsf{T} R\mathbf{r} + \mathbf{v}^\mathsf{T}\mathbf{r}\right)\\
&\qquad = \partial_\mathbf{v} B^\mathsf{T} K A \partial_{\mathbf{v}^\mathsf{T}} \langle B, \mathbf{b}|A, \mathbf{a}\rangle.
\end{aligned} \tag{A.24}$$

By direct calculation using (2.17), the product rule and identity (A.4)

$$\begin{aligned}
&\partial_\mathbf{v} B^\mathsf{T} K A \partial_{\mathbf{v}^\mathsf{T}} \langle B, \mathbf{b}|A, \mathbf{a}\rangle\\
&\qquad = \partial_\mathbf{v} B^\mathsf{T} K A \partial_{\mathbf{r}^\mathsf{T}} \exp\left(\frac{1}{4}\mathbf{v}^\mathsf{T} R\mathbf{v}\right) M_0\\
&\qquad = \frac{1}{2}\partial_\mathbf{v} B^\mathsf{T} K A R\mathbf{v} \exp\left(\frac{1}{4}\mathbf{v}^\mathsf{T} R\mathbf{v}\right) M_0\\
&\qquad = \left[\frac{3}{2}\mathrm{Tr}\left(BKAR\right) + \frac{1}{4}\mathbf{v}^\mathsf{T} RBKAR\mathbf{v}\right] \langle B, \mathbf{b}|A.\mathbf{a}\rangle
\end{aligned} \tag{A.25}$$

Inserting back into (A.21) the total kinetic matrix element

$$\begin{aligned}
&\langle B, \mathbf{b}|\hat{K}|A, \mathbf{a}\rangle =\\
&\qquad \Big[\mathbf{b}^\mathsf{T} K\mathbf{a} - \mathbf{b}^\mathsf{T} KAR\mathbf{v} - \mathbf{v}^\mathsf{T} RBK\mathbf{a}\\
&\qquad\quad + 6\mathrm{Tr}\left(BKAR\right) + \mathbf{v}^\mathsf{T} RBKAR\mathbf{v}\Big] \langle B, \mathbf{b}|A\mathbf{a}\rangle,
\end{aligned} \tag{A.26}$$

which reduces to

$$= \left[6\mathrm{Tr}\left(BKAR\right) + \left(\mathbf{b} - BR\mathbf{v}\right)^\mathsf{T} K(\mathbf{a} - AR\mathbf{v})\right] \langle B, \mathbf{b}|A, \mathbf{a}\rangle. \tag{A.27}$$

In the case of s-waves we let $\mathbf{a} = \mathbf{b} = 0 \Rightarrow \mathbf{v} = 0$ such that

$$\langle B|\hat{K}|A\rangle \overset{\mathbf{v}}{=} {}^{\to} {}^{0}\, 6\mathrm{Tr}\left(BKAR\right) M_0 \tag{A.28}$$

## Harmonic Oscillator Matrix Element

We are also interested in the expectation value of the harmonic oscillator. The harmonic oscillator is proportional to the $r^2$, and the operator i question can thus be expressed as [12]

$$V\left(w^T\mathbf{r}\right) \propto \mathbf{r}^T w w^T \mathbf{r}. \tag{A.29}$$

The matrix element become

$$\begin{aligned}\langle B, \mathbf{b}|\mathbf{r}^\mathsf{T} w w^\mathsf{T} \mathbf{r}|A, \mathbf{a}\rangle \\ &= \int d^3\vec{r}_1, d^3\vec{r}_2, ..., d^3\vec{r}_N \langle B, \mathbf{b}|\mathbf{r}\rangle \mathbf{r}^T w w^T \mathbf{r} \langle \mathbf{r}|A, \mathbf{a}\rangle \\ &= \int d^3\vec{r}_1, d^3\vec{r}_2, ..., d^3\vec{r}_N \mathbf{r}^\mathsf{T} w w^\mathsf{T} \mathbf{r} \exp\left(-\mathbf{r}^\mathsf{T} R \mathbf{r} + \mathbf{v}^\mathsf{T}\mathbf{r}\right),\end{aligned} \tag{A.30}$$

where $R = B + A$ and $\mathbf{v}^T = \mathbf{a}^T + \mathbf{b}^T$. The integral can be rewritten in terms of derivatives of the shift vectors

$$\begin{aligned}&= \int d^3\vec{r}_1, d^3\vec{r}_2, ..., d^3\vec{r}_N \partial_\mathbf{v} w w^\mathsf{T} \partial_{\mathbf{v}^\mathsf{T}} \exp\left(-\mathbf{r}^\mathsf{T} R \mathbf{r} + \mathbf{v}^\mathsf{T}\mathbf{r}\right) \\ &= \partial_\mathbf{v} w w^\mathsf{T} \partial_{\mathbf{v}^\mathsf{T}} \int d^3\vec{r}_1, d^3\vec{r}_2, ..., d^3\vec{r}_N \exp\left(-\mathbf{r}^\mathsf{T} R \mathbf{r} + \mathbf{v}^\mathsf{T}\mathbf{r}\right).\end{aligned} \tag{A.31}$$

The last integral is simply the overlap, such that

$$\begin{aligned}&= \partial_\mathbf{v} w w^\mathsf{T} \partial_{\mathbf{v}^\mathsf{T}} \langle B, \mathbf{b}|A, \mathbf{a}\rangle \\ &= \partial_\mathbf{v} w w^\mathsf{T} \partial_{\mathbf{v}^\mathsf{T}} \exp\left(\frac{1}{4}\mathbf{v}^\mathsf{T} R \mathbf{v}\right) M_0,\end{aligned} \tag{A.32}$$

where we have used Eq. (2.17) in the last line. This calculation is similar to one considered in the derivation of the kinetic matrix element. We apply the product rule with identities (A.3) and (A.2)

$$\begin{aligned}\langle B, \mathbf{b}|\mathbf{r}^\mathsf{T} w w^\mathsf{T} \mathbf{r}|A, \mathbf{a}\rangle \\ &= \left[\frac{3}{2}\mathrm{Tr}(w w^\mathsf{T} R) + \frac{1}{4}\mathbf{v}^\mathsf{T} R w w^\mathsf{T} R \mathbf{v}\right] \langle B, \mathbf{b}|A, \mathbf{a}\rangle \\ &= \left[\frac{3}{2} w^\mathsf{T} R w + \frac{1}{4}\mathbf{v}^\mathsf{T} R w w^\mathsf{T} R \mathbf{v}\right] \langle B, \mathbf{b}|A, \mathbf{a}\rangle,\end{aligned} \tag{A.33}$$

where the last step can be seen by expanding into component form[4]. For s-waves we let $\mathbf{v} \to 0$

$$\langle B|\mathbf{r}^\mathsf{T} w w^\mathsf{T} \mathbf{r}|A\rangle \overset{\mathbf{v}\to 0}{=} \frac{3}{2}\left(w^\mathsf{T} R w\right) M_0. \tag{A.34}$$

4 There is an implicit sum over repeated indices

$$\mathrm{Tr}(w w^\mathsf{T} R) = \left(w w^\mathsf{T} R\right)_{ii} = \left(w w^\mathsf{T}\right)_{ij} R_{ji} = w_i w_j R_{ji} = w^\mathsf{T} R w$$

## Gaussian Matrix Element

The Gaussian type formfactor can be written in the following form

$$V(w^{\mathsf{T}}\mathbf{r})\exp\left(-\alpha\mathbf{r}^{\mathsf{T}}ww^{\mathsf{T}}\mathbf{r}\right)|. \tag{A.35}$$

The resulting matrix element can thus be written as

$$\begin{aligned}\langle B,\mathbf{b}|\exp\left(-\alpha\mathbf{r}^{\mathsf{T}}ww^{\mathsf{T}}\mathbf{r}\right)|A,\mathbf{b}\rangle \\ = \int d\vec{r}_1^3, d\vec{r}_2^3,\ldots,d\vec{r}_N^3\langle B,\mathbf{b}|\mathbf{r}\rangle\exp\left(-\alpha\mathbf{r}^{\mathsf{T}}ww^{\mathsf{T}}\mathbf{r}\right)\langle\mathbf{r}|A,\mathbf{a}\rangle\end{aligned} \tag{A.36}$$

$$\begin{aligned}= \int d\vec{r}_1^3, d\vec{r}_2^3,\ldots,d\vec{r}_N^3\exp\left(\mathbf{r}^{\mathsf{T}}B\mathbf{r}+\mathbf{b}^{\mathsf{T}}\mathbf{r}\right) \\ \times\exp\left(-\alpha\mathbf{r}^{\mathsf{T}}ww^{\mathsf{T}}\mathbf{r}\right)\exp\left(\mathbf{r}^{\mathsf{T}}A\mathbf{r}+\mathbf{a}^{\mathsf{T}}\mathbf{r}\right),\end{aligned} \tag{A.37}$$

which we can neatly assemble into a single Gaussian

$$\begin{aligned}&= \int d\vec{r}_1^3, d\vec{r}_2^3,\ldots,d\vec{r}_N^3\exp\left(\mathbf{r}^{\mathsf{T}}(B+A+\alpha ww^{\mathsf{T}})\mathbf{r}+\mathbf{v}^{\mathsf{T}}\mathbf{r}\right) \\ &= \langle B+A\alpha ww^{\mathsf{T}},\mathbf{b}|A,\mathbf{a}\rangle.\end{aligned} \tag{A.38}$$

From the result for the overlap between two Gaussians (2.17), we get the expectation value of a Gaussian form-factor

$$\begin{aligned}\langle B,\mathbf{b}|\exp\left(-\alpha\mathbf{r}^{\mathsf{T}}ww^{\mathsf{T}}\mathbf{r}\right)|A,\mathbf{b}\rangle \\ = \exp\left(\frac{1}{4}\mathbf{v}^{\mathsf{T}}(B+A+\alpha ww^{\mathsf{T}})^{-1}\mathbf{v}\right)\left(\frac{\pi^N}{\det((B+A+\alpha ww^{\mathsf{T}}))}\right)^{\frac{3}{2}}.\end{aligned} \tag{A.39}$$

For s-waves we let $\mathbf{v}\to 0$

$$\langle B|\exp\left(-\alpha\mathbf{r}^{\mathsf{T}}ww^{\mathsf{T}}\mathbf{r}\right)|A\rangle \overset{\mathbf{v}\to 0}{=} \left(\frac{\pi^N}{\det((B+A+\alpha ww^{\mathsf{T}}))}\right)^{\frac{3}{2}}. \tag{A.40}$$

# APPENDIX B

# Deuteron with Gaussian Potential

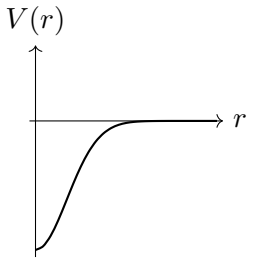


Figure B.1: Shape of the Gaussian potential.

The recipe was also tested against a Gaussian interaction model (see Figure B.1) to calculate the associated scattering parameters. The Gaussian potential is given as [20]

$$W(r) = -V_0 \exp\left(-\frac{r^2}{r_n^2}\right), \tag{B.1}$$

with parameters $V_0 = 72.5$ MeV and $r_n = 1.47$ fm. We shall use the nucleon masses from [20], such that $m_n = 939.508$ MeV and $m_p = 938.214$ MeV. As there is no bound state of the deuteron singlet, we will target the nucleon-nucleon triplet state, for which the reported values for the scattering length and effective range parameter is [20]

$$a_t = 5.38 \pm 0.03 \text{ fm}, \qquad r_e = 1.71 \pm 0.03 \text{ fm}. \tag{B.2}$$

The system is placed in an artificial oscillator potential in accordance with the prescribed recipe. In relative Jacobi coordinates, the corresponding Schrödinger equation reads

$$\begin{aligned}\Bigg[ -\frac{\partial}{\partial \mathbf{r}_{\text{pn}}} K' \frac{\partial}{\partial \mathbf{r}_{\text{np}}^{\mathsf{T}}} + V_0 \exp\left(-\frac{\mathbf{r}_{\text{np}}^{\mathsf{T}} \tilde{w}_{\text{np}} \tilde{w}_{\text{np}}^{\mathsf{T}} \mathbf{r}_{\text{np}}}{r_n^2}\right) \\ + \frac{1}{4}\frac{\hbar^2}{2\mu b_{\text{o}}^4}(\mathbf{r}_{\text{np}}^{\mathsf{T}} \tilde{w}_{\text{osc}} \tilde{w}_{\text{osc}}^{\mathsf{T}} \mathbf{r}_{\text{np}})\Bigg] \Psi = E\Psi.\end{aligned} \tag{B.3}$$

The wave function is expanded in a basis of correlated Gaussians, the parameters of which are optimised by minimising the sum of the ground

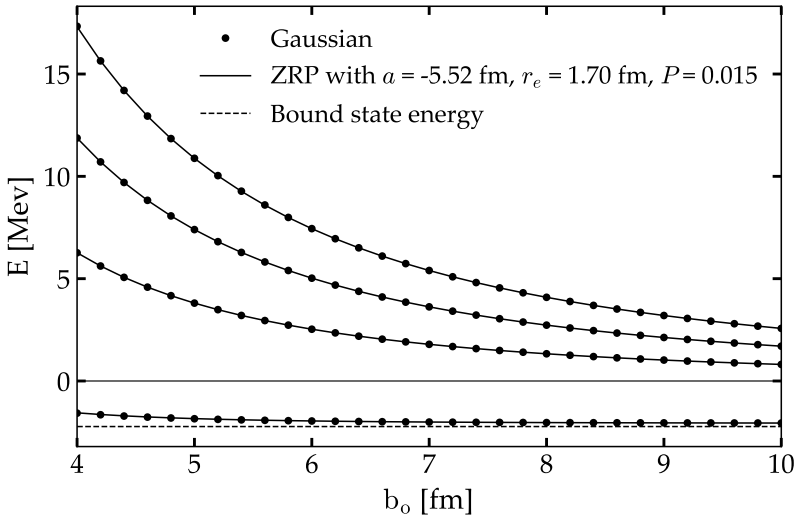


Figure B.2: Gaussian interaction model plotted against the zero-range model; The dots show the spectrum for a deuteron in a Gaussian potential and an oscillator trap. The solid lines show the eigenenergy spectrum of the same particle in the trap interacting with a ZRP, Eq. (3.17), with parameters $a = -5.52$, $r_e = 1.70$ and $P = 0.015$. The dashed line indicate the bound state energy of the deuteron [20]. The threshold of the system is at 0

and 1st excited state. The spectrum of Eq. (B.3) is calculated numerically for a range of trap sizes, $b_o$. This is shown in figure B.2. To get a sense of the agreement between the models, the ZRP-model – with the fitted model parameters – is plotted on top as indicated by the solid lines. As was the case for the Volkov potential, the agreement between the models is very good, with the ZRP-model able to reproduce the spectrum of the four levels close to threshold.

However, the extracted scattering length overestimates the reported value in [20]. This discrepancy might be partly due to variations in the value of $\hbar c$, which was not declared in [20]. The values of the extracted parameters are quite susceptible, even to small changes in $\hbar c$. The convergence as a function of trap size is depicted in Figure B.3.

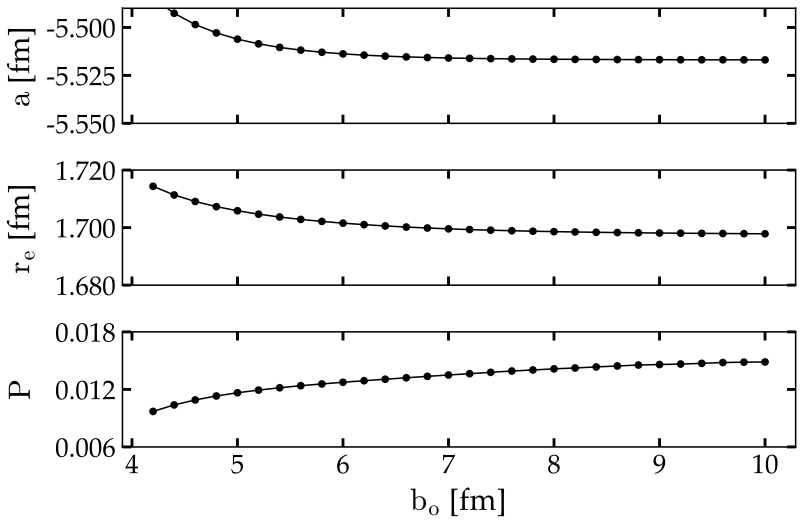


Figure B.3: Convergence of scattering parameters as a function of trap range. Each point represents the parameter fitted across the energies of the preceding two fermi. The solid line serves to indicate the trend of the convergence

APPENDIX C

# Significance of the 3rd Order Term

Figure C.1 shows the convergence as a function of trap size for a deuteron in a Volkov potential for the 2nd and 3rd order expansion of Eq. (3.17). As evident from the figure, the 3rd order expansion (the black curves) converges faster than the 2nd order expansion, allowing for a smaller value of $b_o$ in the calculated spectrum.

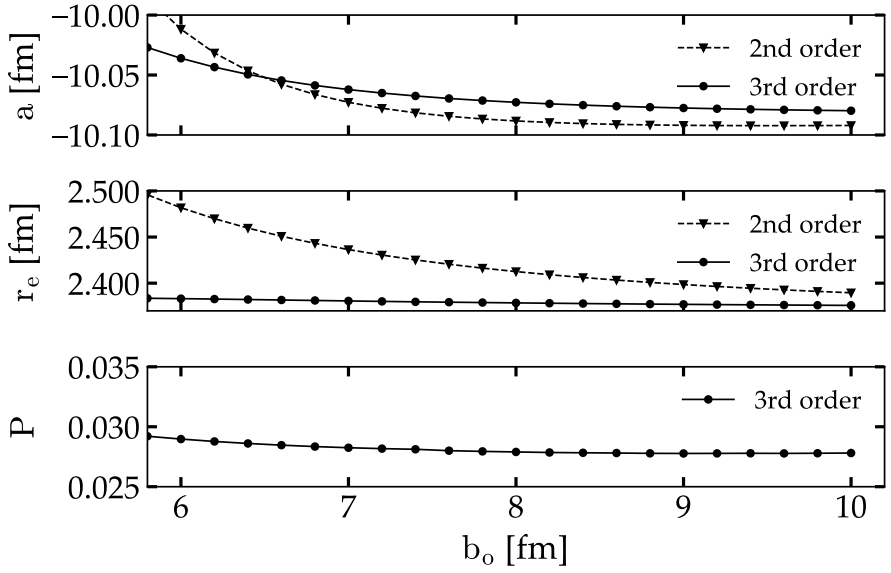


Figure C.1: Comparison of convergence trends for the 2nd and 3rd order parameters calculated from the zero-range formula Eq. (3.17).